STUDY ON NANOSTRUCTUED METAL NANOPARTICLES/NANOCLUSTERS ENHANCED ORGANIC THIN-FILM SOLARCELLS

APICHAT PANGDAM

DOCTORAL PROGRAM IN ELECTRICAL AND INFORMATION ENGINEERING
GRADUATE SCHOOL OF SCIENCE AND TECHNOLOGY
NIIGATA UNIVERSITY

ABSTRACT

Thin-film organic solar cells (OSCs) were fabricated by assembly of thin-film organic layers with different activities for photovoltaic process. The challenge of OSCs is economical cost, thin-film structure, and fixable substrate. However, the disadvantage of OSCs such as high reflection and low absorption of solar light due to the design of OSCs gives the percent of solar cell efficiency (%PCE) less than it should be. Therefore, increasing %PCE is important topic. By the fabrication of nanoscale structure with variety of metal nanoparticles (*i.e.* silver and gold nanoparticles (AgNPs and AuNPs)), plasmonic and fluorescence properties were produced and controlled. The plasmonic and fluorescence properties of metal nanoparticles have been used as a light-trapping and light-converting material, respectively, while the thickness of each layer in OSCs is still constant.

In our work, the plasmonic enhancement of urchin-like gold nanoparticles (UL-AuNPs) and combination of different plasmonic excitations of silver nanoprisms (mixed-AgNPrs) shows the promising evident for light absorption and light scattering in broadband wavelength in visible range that improve solar cell efficiency. However, plasmonic properties of AuNPs and AgNPs are limited in visible light (400-800 nm). To open another opportunity, gold quantum dots (AuQDs) are used for harvesting UV light and converting to visible light for OSC. By plasmonic and fluorescence enhancement, %PCE of developing OSCs were increased by 5 – 10% when compared with the reference cell. All of metal nanoparticles (*i.e.* UL-AuNPs, Mixed-AgNPrs and AuQDs) were included in a hole transport layer of OSCs.

Furthermore, the aggregation of metal nanoparticles on the hole transport layer and effect to photovoltaic parameters were investigated by UV-vis spectroscopy, atomic force microscope, J-V characteristic, and impedance spectroscopy. The concentration of metal nanoparticles plays an important role to control a aggregation degree on hole transport layer film. This phenomenon induces the plasmonic or fluorescence quenching and generates short-

circuit current that reduce %PCE of OSCs. Moreover, the mechanism of plasmonic or fluorescence enhancement from metal nanoparticles were observed by incident photon-to-current and supported by finite-difference time-domain simulation.

KEYWORDS: Urchin-like gold nanoparticles, Gold quantum dots, Silver nanoprisms, Light-trapping materials, Light-converting materials, Fluorescence materials, FDTD and Plasmonic materials

ACKNOWLEDGMENTS

I would like to express my sincere gratitude to my thesis advisors, Associate Professor Dr. Akira Baba who gave me the opportunity to research at Niigata University and gain experience from the knowledge of research group. Moreover, I would like to thank Professor Dr. Sanong Ekgasit for invaluable guidance and suggestions throughout this work.

I wish to express my grateful thank to Professor Dr. Futao Kaneko, Professor Dr. Keizo Kato, Professor Dr. Kazunari Shinbo, Assistance Professor Dr. Ryousuke Ishikawa, and Assistance Professor Dr. Chutiparn Lertvachirapaiboon from Niigata University and Associate Professor Chuchaat Thammacharoen and Assistance Professor Dr. Kanet Wongravee from Chulalongkorn University for their valuable advice.

Warmest thanks to my friend, my colleagues and organization: Center for Transdisciplinary Research, Niigata University, and all good friends for suggestion and spiritual supports throughout this research. Also they provide the good experience for me about Japanese culture which will broaden my horizon in different work culture for developing my research career in the future.

The financial support from The “Global Circus” Program of Niigata University supported by the Ministry of Education, Culture, Sports, Science and Technology.

Above all, I am profoundly grateful to my parents and endearing family for all their loves, understanding, support, and encouragement during the whole period of my study.

CONTENTS

CONTENTS

CONTENTS

Page

LIST OF FIGURE

Figure Page

CHAPTER I INTRODUCTION

CHAPTER II Effect of urchin-like gold nanoparticles in organic thin-film solar cells

LIST OF FIGURE

Figure Page

CHAPTER III Investigation of gold quantum dots enhanced organic thin film solar cells

LIST OF FIGURE

Figure Page

LIST OF FIGURE

Figure Page

CHAPTER IV Enhanced organic thin-film solar cell efficiency via the combination of three difference plasmonic excitations of silver nanoprisms

LIST OF FIGURE

Figure Page

LIST OF ABBREVIATIONS

LSPR	Localized surface plasmon resonance
CCD	Central composition design
MLR	Multiple liner regression
PL	Photoluminescent
QY	Quantum yield
UV	Ultraviolet
OSCs	Thin film organic solar cells
AL	Active layer
HTL	Hole transport layer
ETL	Electron transport layer
LUMO	Lowest unoccupied molecular orbital
HOMO	Highest occupied molecular orbital
%PCE	Percent of Power Conversion Efficiency
FDTD	Finite-difference time-domain
IPCE	Incident photon to current efficiency
R_s	Series resistance
R_{sh}	Short resistance
R_{ct}	Charge transfer resistance
CPE	Constant phase element
E.F.	Enhancement factor
J_{sc}	Short-circuit current density
V_{oc}	Open-circuit voltage
FF	Fill factor
P_m	Maximum power

J_m	Current density
V_m	Voltage
P_{in}	Incident photon power
AM	Air mass
AuNPs	Gold nanoparticles
AgNPs	Silver nanoparticles
QDs	Quantum dots
P3HT	Poly(3-hexylthiophene)
PCBM	Phenyl-C61-butyric acid methyl ester
PEDOT:PSS	Poly(3,4-ethylenedioxythiophene) polystyrene sulfonate
AFM	Atomic force microscope
TEM	Transmission electron microscope
UL-AuNPs	Urchin-like gold nanoparticles
AuQDs	Gold quantum dots
AgNPrs	Silver nanoprisms

CHAPTER I

INTRODUCTION

RESEARCH BACKGROUND

Thin film organic solar cells (OSCs)

Thin film organic solar cells (OSCs) are a bulk heterojunction organic semiconductor for producing electricity by photovoltaic process. Recently, OSCs are developed, and the percent of power conversion efficiency (%PCE) is continuously increased to 6% and 10% in tandem cells.[1] The outstanding properties of OSCs such as economical and flexible photovoltaic cells based on organic materials influenced researcher to develop and improve more %PCE in future.[2] The OSCs have many architectural designs as shown in Figure 1 such as conventional cell (a), inverted cell (b) and tandem cell (c and d). These OSCs have contained with many layers in devices such as anode, cathode, active layer (AL) and hole transport layer (HTL) or electron transport layer (ETL) depended on type of OSCs.

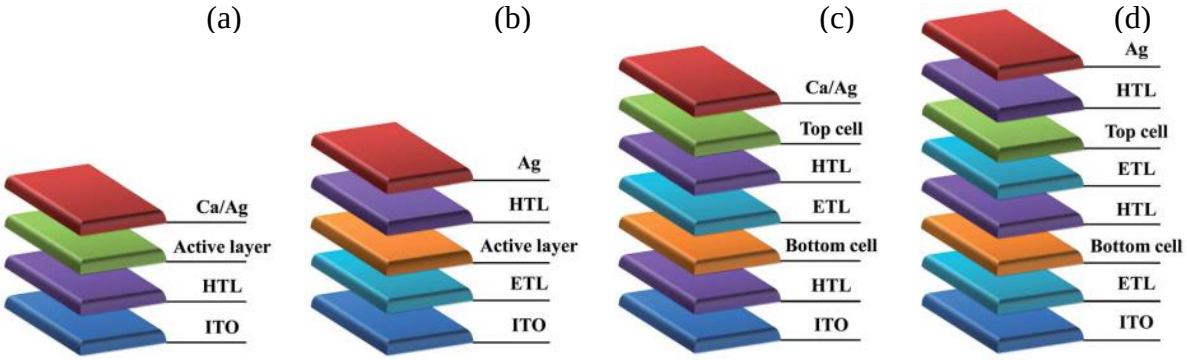

Figure 1 Diagram of conventional organic thin-film photovoltaic cell. [3] Copyright 2013 Royal Society of Chemistry.

The main part in OSCs is the active layer (AL) due to photovoltaic phenomena occurring in this layer. Figure 2 shows that the electricity was generated by the diffusion of electron-hole pair from AL to electrode under photo irradiations. Briefly, when bulk-heterojunction

polymer solar cells were excited by photon. The photo-induced excitons and electron diffuse to lowest unoccupied molecular orbital (LUMO) of donor (D) and accept (A) organic molecule (1 & 1′), respectively. In the same time, the hole relocates to highest occupied molecular orbital (HOMO) of D and A (2 & 2′). Afterward, electron and hole move to cathode (3, 4, 5 & 6) and anode (3′, 4′, 5′ & 6′), respectively. These phenomena could drive the electric current to flow in the circuit.[4]

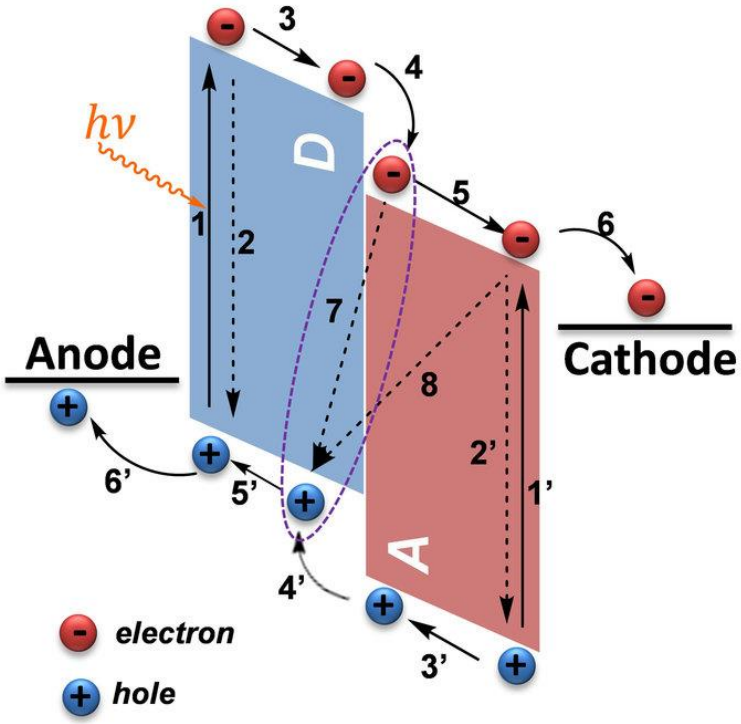

Figure 2 The schematic of the photoinduced charge transfer of donor to accepter organic molecule in photovoltaic system. [4]

To date, the active layer (AL) has been achieved based on polymer donors and fullerene acceptors. Figure 3 shows some example of organic semiconductor as doners (p-type polymers) and acceptors (n-type polymers).[5] These materials are selected to use by considering the range of light absortion and energy level of each chemical. The energy level in organic solar cells plays an important role for the charge tranfer in photovotaic phemomenars.

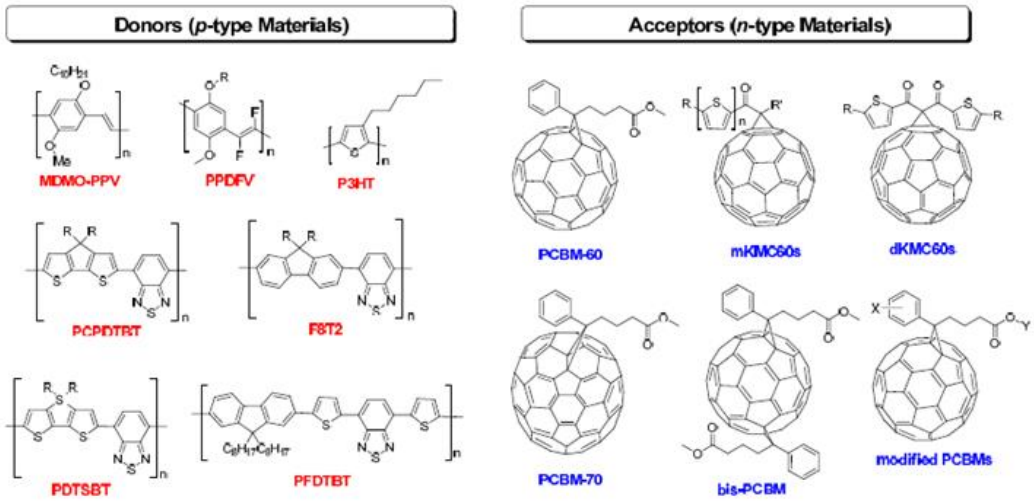

Figure 3 the chemical structures of donor and acceptor organic molecule for OSCs. [6]

The power conversion efficiency (PCE) is necessary value for considering or comparing in solar cell development research. The %PCE of OSCs is calculated by three parameters such as short-circuit current density (J_{SC}), open-circuit voltage (V_{OC}) and fill factor (FF).[7] Figure 4 shows the current–voltage (J–V) curves of a typical OSC under dark and illumination.

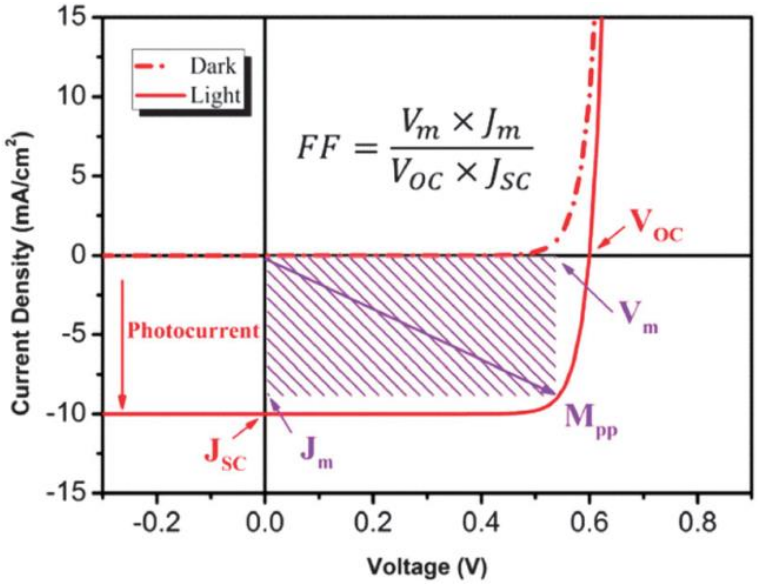

Figure 4 The current–voltage characteristics for dark and light current in a solar cell. [7] Copyright 2013 Royal Society of Chemistry.

Especially, the maximum power (P_m) is oocured with the current density and voltage as J_m and V_m , then the percent of solar cell efficency (%η) can be calculated by:

$$\eta = \frac{P_m}{P_{in}} = \frac{J_m V_m}{P_{in}} = \frac{J_{SC} V_{OC} FF}{P_{in}}$$

When P_{in} is the incident photon power on the device, and FF is calculated by:

$$FF = \frac{P_m}{J_{SC} V_{OC}} = \frac{J_m V_m}{J_{SC} V_{OC}}$$

Light-harvesting for OSCs

The thin-film structures and flat surface of OSCs have several problems in terms of high light reflection on top surface and low light absorption within AL, respectively. These are mainly causes for reducing incident photon and converting sunlight to electricity.[8] To consider the solar spectrum, OSCs can absorb light only the visible region around 400 – 800 nm that is 53% of total solar power as shown in Figure 5.[9] Light-harvesting technique could increase the light absorption in visible regions for rising the excitons of donor and accepter polymer and also % PCE within OSCs. Many researches show the ideas to reduce an optical loss or induce a excitons activity such anti-reflection coating[10], plasmonic materials[11] and luminescent solar concentrator[12].

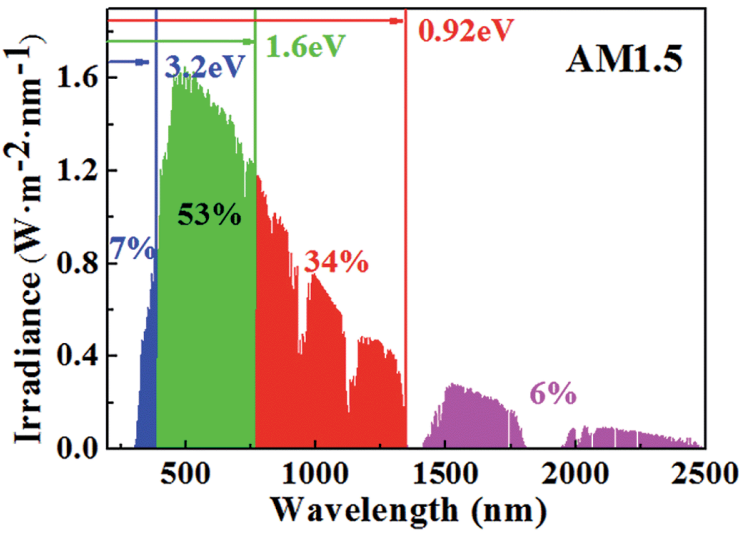

Figure 5 The solar spectrum at AM1.5. [9] Copyright 2014 Royal Society of Chemistry.

Gold and silver particles for light-harvesting in OSCs

1. Novel properties by quantum-size-effect

Reducing gold and silver particle sizes provides the promising properties that are different from bulk materials. Especially, their optical properties were explained by quantum confinement as shown in Figure 6. The conduction band and valence band of metal particles can be separated when the particles size becomes less than 2 nm, which is called "molecular like" state. The novel properties of plasmonic and fluorescence properties were expected.[13]

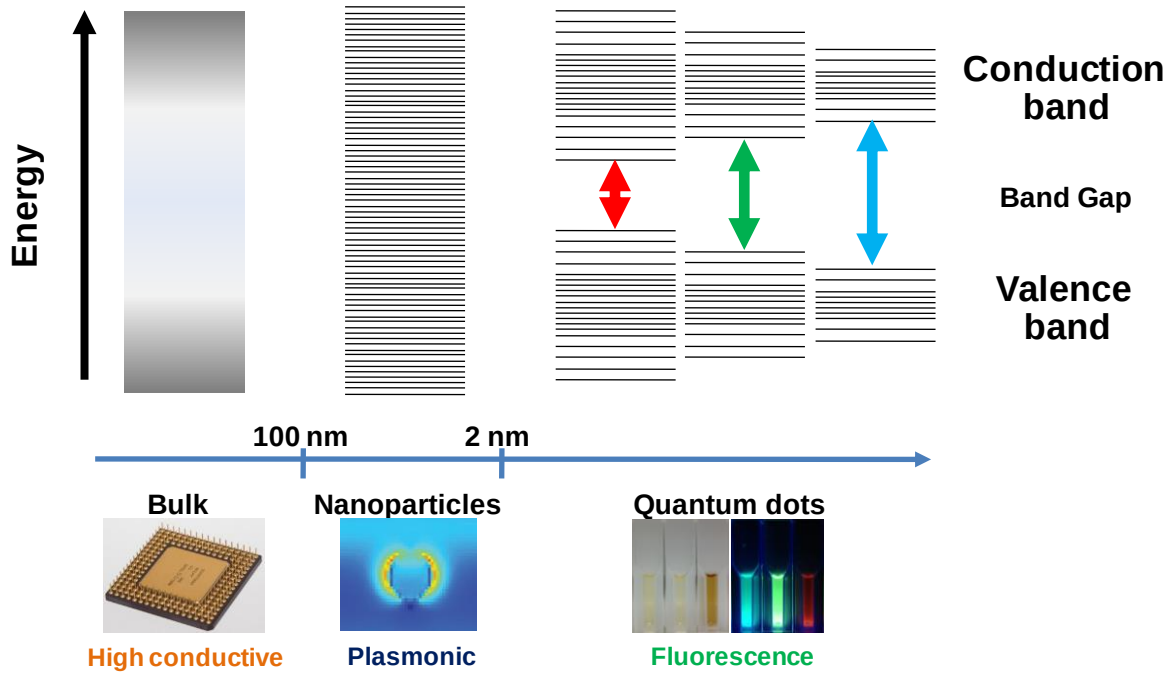

Figure 6 The quantum size effect on band gap energy and specice properties of gold

2. Plasmonic nanomaterials

The plasmonic properties of gold and silver nanoparticles (AuNPs/ AgNPs) were wildly used in many applications such as colorimetric sensor, cancer therapy and trace analysis.[14] The electromagnetic field enhancement of these nanomaterials plays an important role for utilization that can be explained by localized surface plasmon resonance (LSPR) as shown in Figure 7. When incident photon acts with surface of metal nanoparticles and have a similar frequency with electron cloud oscillation on metal surface, then, the resonance frequency

between photon and electron cloud is occurred that results in the storage of energy in the LSPR for metal nanoparticles.[15, 16] The LSPR properties directly depend on morphology (particle size and shape) and surrounding medium.[17]

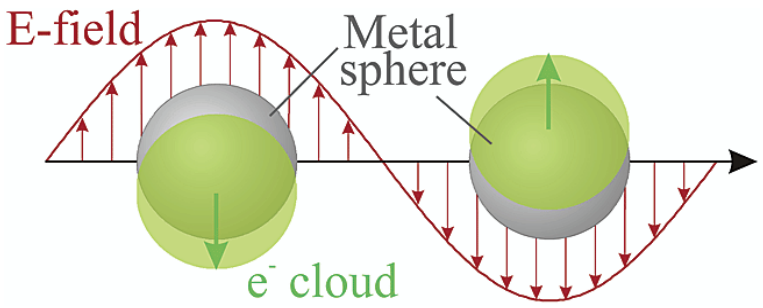

Figure 7 Illustration of electron cloud oscillation for localized surface plasmon resonance (LSPR) of metal nanospheres. [14] Copyright 2003 American Chemical Society.

In the case of OSCs as shown in Figure 8, AuNPs, AgNPs demonstrate for improving the light absorption owning to LSPR, which generates local electromagnetic field of the plasmonic solar cells.[11] In addition, the incident photons scatter and propagate within solar cells by metallic nanostructures that ca be explained by Mie scattering. These features potentially enhance the light absorption and photocurrent generation for active layers of OSCs.[18]

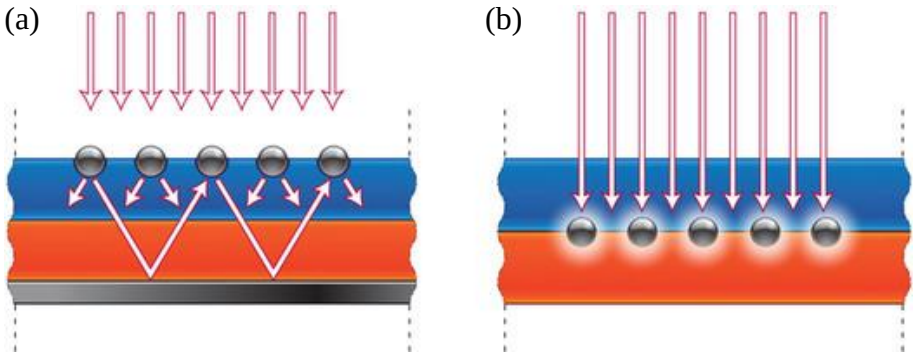

Figure 8 Plasmonic light-trapping architecture for thin-film solar cells, scattering mode by metal nanoparticles (A), LSPR excitation mode by metal nanoparticles (B). [11] Copyright 2010 Nature Publishing Group

3. Quantum dot fluorescence

The conduction and valence bands of quantum dots (QDs) are suitable to accumulate non-radiative relaxation in valence band affected by quantum size effect. Therefore, when electrons in conduction band are excited by high-energy photon, the luminescent photon can emit to low-energy photon as shown in Figure 9.[19] The semiconductor nanocrystals or QDs should have the size as small as 2 to 10 nanometers.[20] In the case of gold and silver nanocrystals, gold quantum dots (AuQDs) can show remarkable size-tunable photoluminescence when the size is less than 2 nm.[21] However, silver quantum dots (AgQDs) did not show strong evident for light emission.[22-24] The novel spectroscopic properties of QDs are size-tunable photoluminescent (PL) emission and high quantum yield (QY), which can apply in many fields such as sensor, medical device and solar cells.

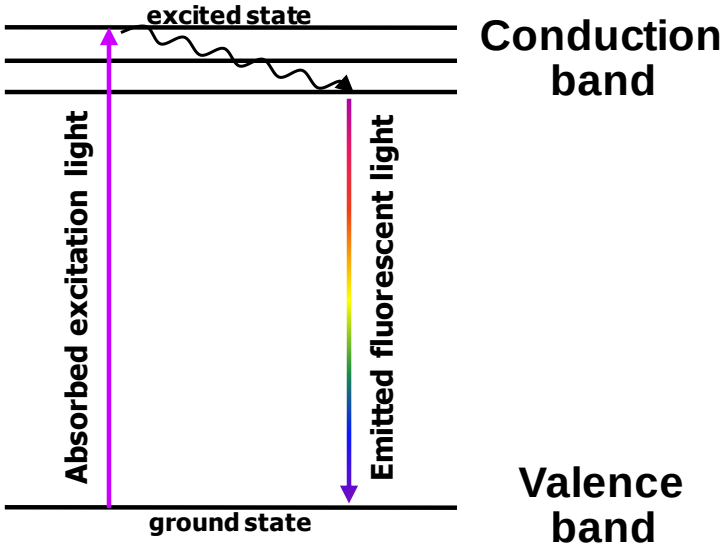

Figure 9. Fluorescence or luminescence diagram shows the electron excitation from valence band to conduction band and relief as fluorescence light.

In the case of solar cells, QDs were used as a photosensitizer for light-harvesting of sensitized solar cells.[19] Moreover, QDs were used in OSCs for improving the photocurrent in the visible range; the materials absorbed and emitted UV and visible light, respectively,

due to the quantum effect of the semiconductor QDs.[25] This idea supports using QDs for light-converting materials and increasing photocarriers in OSCs.

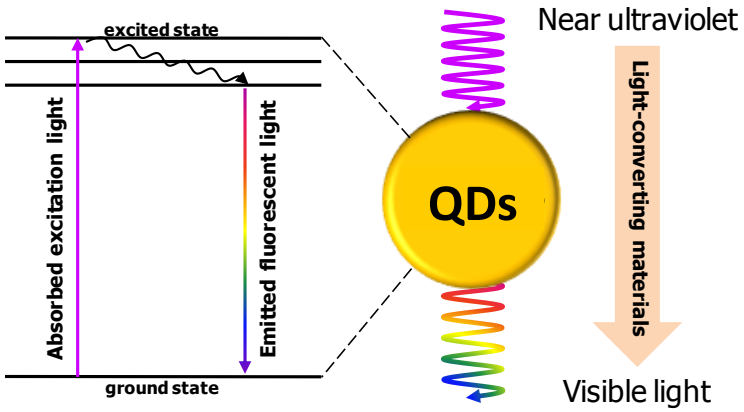

Figure. 10 QDs for light-converting idea to convert UV to visible light.

OBJECTIVES

To harvest the broadband solar light, the plasmonic and fluorescence properties of gold and silver nanoparticles were used for light trapping in organic thin-film solar cells. For enhancement of solar cells efficiency, gold and silver nanoparticles are necessary to be synthesize and design for plasmonic and fluorescence tuning with several light absorption from UV to visible region. Therefore, major aims of this thesis are:

1. To synthesize gold nanoparticles by structural control synthesis for the broadband light absorption for OSCs
2. To study of gold quantum dots in difference size and shape for light converting form UV to visible for OSCs
3. To mix silver nanoparticles in difference size and shape for making broadband light absorption for OSCc

SCOPE OF THE DISSERTATION

The light tapping by gold and silver nanoparticles was studied in OSCs. The poly(3-hexylthiophene) (P3HT) and phenyl-C61-butyric acid methyl ester (PCBM) were used as active layer, and poly(3,4-ethylenedioxythiophene) doped with poly(styrene sulfonate) were used as hole transport layer of OSCs. The conventional structure of OSCs as follows: ITO(anode)/PEDOT:PSS/P3HT:PCBM/Al(cathode) were fabricated in this investigation. Gold and silver nanoparticles were included in hole transport layer. The effect of plasmonic and fluorescence from these nanoparticles in OSCs were observed by UV-visible spectrum, J-V curve, surface morphology, impedance spectrum and incident photon to current efficiency. Therefore, three work chapters are included as follows:

1. Effect of urchin-like gold nanoparticles in organic thin-film solar cells
2. Investigation of gold quantum dots enhanced organic thin film solar cells
3. Enhanced organic thin-film solar cell efficiency via the combination of three difference plasmonic excitations of silver nanoprisms

REFERENCES

1. J. You, L. Dou, Z. Hong, G. Li and Y. Yang, *Prog. Polym. Sci.*, 2013, **38**, 1909-1928.
2. C. C. Chen, L. Dou, J. Gao, W. H. Chang, G. Li and Y. Yang, *Energ. Environ. Sci.*, 2013, **6**, 2714-2720.
3. N. Li, D. Baran, K. Forberich, F. Machui, T. Ameri, M. Turbiez, M. Carrasco-Orozco, M. Drees, A. Facchetti, F. C. Krebs and C. J. Brabec, *Energ. Environ. Sci.*, 2013, **6**, 3407-3413.
4. K. Wang, C. Yi, C. Liu, X. Hu, S. Chuang and X. Gong, *Sci. Rep.*, 2015, **5**, 9265.
5. Y. J. Cheng, S. H. Yang and C. S. Hsu, *Chem. Rev.*, 2009, **109**, 5868-5923.
6. A. M. Bagher, *Sustainable Energy*, 2014, **2**, 85-90.

7. B. Qi and J. Wang, *Phys. Chem. Chem. Phys*., 2013, **15**, 8972-8982.
8. Z. Tang, W. Tress and O. Inganäs, *Mater. Today*, 2014, **17**, 389-396.
9. Z. Wu, W. Wang, Y. Cao, J. He, Q. Luo, W. A. Bhutto, S. Li and J. Kang, *J. Mater. Chem. A*, 2014, **2**, 14571-14576.
10. J. Cai and L. Qi, *Mater. Horiz.*, 2015, **2**, 37-53.
11. H. A. Atwater and A. Polman, *Nat Mater*, 2010, **9**, 205-213.
12. F. Purcell-Milton and Y. K. Gun'ko, *J. Mater. Chem.*, 2012, **22**, 16687-16697.
13. C. L. C. Smith, N. Stenger, A. Kristensen, N. A. Mortensen and S. I. Bozhevolnyi, *Nanoscale*, 2015, **7**, 9355-9386.
14. K. L. Kelly, E. Coronado, L. L. Zhao and G. C. Schatz, *J. Phy. Chem. B*, 2003, **107**, 668-677.
15. K. M. Mayer and J. H. Hafner, *Chem. Rev*., 2011, **111**, 3828-3857.
16. K. A. Willets and R. P. V. Duyne, Annu. *Rev. Phys. Chem.*, 2007, **58**, 267-297.
17. D. Mustafa, T. Yang, Z. Xuan, S. Chen, H. Tu and A. Zhang, Plasmonics, 2010, **5**, 221-231.
18. E. Stratakis and E. Kymakis, *Mater. Today*, 2013, **16**, 133-146.
19. G. H. Carey, A. L. Abdelhady, Z. Ning, S. M. Thon, O. M. Bakr and E. H. Sargent, *Chem. Rev.*, 2015, **115**, 12732-12763.
20. K. Sapsford, T. Pons, I. Medintz and H. Mattoussi, *Sensors*, 2006, **6**, 925.
21. N. Sakai and T. Tatsuma, *Adv. Mater.*, 2010, **22**, 3185-3188.
22. Z. Lian, W. Wang, S. Xiao, X. Li, Y. Cui, D. Zhang, G. Li and H. Li, *Sci. Rep*., 2015, **5**, 10461.
23. W. Wang and S. A. Asher, *J. Am. Chem. Soc.*, 2001, **123**, 12528-12535.

24. H. Choi, S.-J. Ko, Y. Choi, P. Joo, T. Kim, B. R. Lee, J.-W. Jung, H. J. Choi, M. Cha, J.-R. Jeong, I.-W. Hwang, M. H. Song, B.-S. Kim and J. Y. Kim, *Nat. Photon.*, 2013, **7**, 732-738.

25. Z. Li, X. Zhang, C. Liu, Z. Zhang, Y. He, J. Li, L. Shen, W. Guo and S. Ruan, *J. Phy. Chem. C*, 2015, **119**, 26747-26752.

CHAPTER II

Effect of urchin-like gold nanoparticles in organic thin-film solar cells

Ref.: A. Pangdam et al. Phys. Chem. Chem. Phys. 18, 18500-18506, 2016.

ABSTRACT

In this study, urchin-like gold nanoparticles (UL-AuNPs) are used in the fabrication of organic thin-film solar cells (OSCs). UL-AuNPs, which have gold nanothorns on their surface, enhance light accumulation by acting as light-trapping materials. This is due to the enhanced electric field and light scattering attributed to the nanothorns on the surface of the nanoparticles. UL-AuNPs were incorporated into a poly(3,4ethylenedioxythiophene): poly(styrene sulfonate) (PEDOT:PSS) thin-film layer of organic thin-film solar cells (OSCs). UV-vis spectra, atomic force microscopy (AFM) images, current density versus voltage properties, and the impedance spectra of the fabricated devices were recorded at various concentrations of UL-AuNPs. We found that the efficiency of the OSCs with UL-AuNPs was not only higher than that of a reference cell without nanoparticles but also higher than that of OSCs with spherical AuNPs. Finite-difference time-domain (FDTD) simulation indicated that the electric field around the UL-AuNPs increased due to the presence of nanothorns.

INTRODUCTION

Organic thin-film solar cells (OSCs) have been widely explored due to their potential applications in inexpensive and flexible photovoltaic cells based on organic materials.[1,2] However, one issue with OSCs is their relatively low efficiency, which is not as high as that of silicon-based solar cells.[3] Because organic materials exhibit a relatively high resistance, their photoelectric conversion layers are typically 100–200 nm thick, resulting in low absorption of photons.[4,5] An important challenge in the advancement of OSCs is enhancing light absorption in organic layers while maintaining their thickness. Many researchers have tried to improve light absorption in OSCs, for example, by tuning the band-gap of conjugated polymers for a broad range of light absorption by chemical synthesis,[6–8] adding an anti-reflection structure on OSCs to reduce light reflection via an imprinting technique,[9–12] and

using the plasmonic properties of gold or silver nanoparticles as light amplifiers by blending them with OSCs.[13–16]

Gold nanoparticles (AuNPs) can be easily dispersed in water and are stable in a oxidation/reduction environment.[17] AuNPs have been widely used in multiple research fields such as in sensors,18–20 solar cells,[21–24] and medicine [25–27] because of their plasmonic properties. In the field of OSCs, AuNPs are blended with a hole transport layer (HTL) or an active layer, which can improve the efficiency of devices. [28,29] Due to an enhanced electric field resulting from localized surface plasmon resonance (LSPR) and light scattering known as Mie scattering, strong light absorption can be obtained in OSCs with AuNPs.[13] Therefore, AuNPs are desirable for use as light-trapping materials in OSCs.[30]

Urchin-like gold nanoparticles (UL-AuNPs) are a type of multi-pod gold nanostructures that possess gold nanothorns on the surface. UL-AuNPs display a wide range of light absorption and scattering properties compared with spherical gold nanoparticles of similar size.[31–33] The application of these structures in the fabrication of gold nanostars and spike-shaped gold nanostructures has been studied, and improvement in the efficiency of OSCs was observed.[34,35] In this study, we used UL-AuNPs, which were synthesized by a wet chemical process, for the application of OSCs. Our results demonstrate that blending UL-AuNPs with the HTL plays an important role in improving the power conversion efficiency by enhancing the electric field and light scattering of OSCs. Furthermore, to understand the experimental results, finite-difference time domain (FDTD) simulations were performed by assuming the structures of the UL-AuNPs and spherical AuNPs in OSCs. FDTD simulations indicate an increased electric field distribution around gold nanothorns, which correlates well with the experimental results.

EXPERIMENTAL SECTION

Synthesis of UL-AuNPs

UL-AuNPs were synthesized without a stabilizer via a one-pot technique with H_2O_2 as a reducing agent. 3 mL of 9 M H_2O_2 (Merck) with 25 μM of $AgNO_3$ (Merck) was poured into a test tube containing 0.3 μL of 0.5 M $HAuCl_4$ (Sigma-Aldrich) and 150 mL of spherical gold nanoseeds (O.D. = 1, average size ~20 nm, Sigma-Aldrich). The yellow $HAuCl_4$ solution transformed into a blue–green solution as UL-AuNPs was added. The final solution concentration was 0.5 mM, after which the UL-AuNPs were further diluted to a preferred concentration using deionized water.

Fabrication of OSCs with UL-AuNPs

Figure 1 depicts a schematic of the fabricated UL-AuNP-enhanced bulk-heterojunction OSCs. To introduce UL-AuNPs into OSCs, UL-AuNPs were diluted to a preferred concentration in deionized water. Subsequently, UL-AuNPs solution was mixed with poly(3,4-ethylenedioxythiophene):poly(styrene sulfonate) (PEDOT:PSS) (Clevios, Heraeus Co.) (1:6 v/v) and blended for 1 h in an ultrasonic bath. PEDOT:PSS, containing UL-AuNPs, was deposited on indium tin oxide substrates (FINE brand, Furuuchi Co. Ltd., 10 Ω/cm^2), as a HTL, by a spin-coating method at 1000 rpm for 1 min. The thickness of PEDOT:PSS films was approximately 100 nm (supporting information, Figure S1). The deposited PEDOT:PSS film was then annealed at 120 °C for 20 min. Phenyl-C61-butyric acid methyl ester (PCBM) (Sigma-Aldrich) blended with poly(3-hexylthiophene) (P3HT) (Sigma-Aldrich), which were dissolved in dichlorobenzene (Sigma-Aldrich) with a P3HT:PCBM mass ratio of 1:0.8, was coated on the PEDOT:PSS layer as an active layer by a spin-coating method at 2000 rpm for 1 min. The P3HT:PCBM films thickness was approximately 100 nm (supporting information, Figure S2). The deposited films were then annealed at 120 °C for 10 min. The top aluminum

electrode (thickness = ~150 nm) of OSCs was deposited on the P3HT:PCBM layer using a vacuum evaporation technique. Finally, fabricated OSCs were annealed at 150 °C for 15 min inside a vacuum chamber.

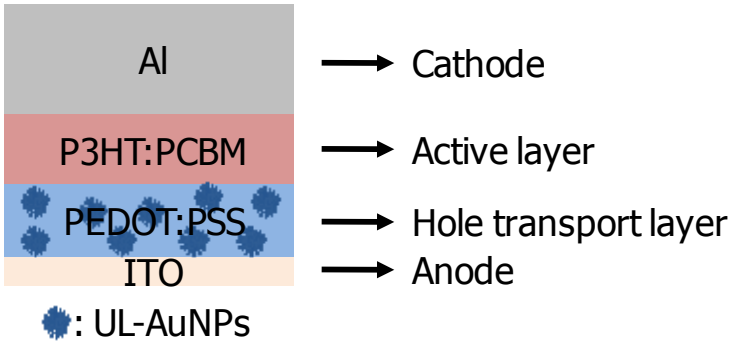

Figure 1. The schematic of fabricated UL-AuNP-enhanced OSC

Characterization of fabricated devices

The UV–vis absorption of PEDOT:PSS and UL-AuNPs-loaded PEDOT:PSS films was measured using a UV–vis spectrometer (V-650, Jasco). The morphology of UL-AuNP dispersions on the surface of PEDOT:PSS films was investigated using atomic force microscope (AFM) (SPM-9600, Shimadzu). Photovoltaic parameters and the impedance spectra of OSCs with and without UL-AuNPs were studied following irradiation under a solar simulator (HAL-C100, 100 W compact xenon light source, Asahi Spectra) equipped with a precision source-meter unit (B2901A, Agilent) and a potentiostat (PARSTAT 4000, Princeton Applied Research).

RESULTS AND DISCUSSION

Effect of UL-AuNPs in UV–vis light absorption

UL-AuNPs display a broad range of light absorption due to plasmonic coupling between the gold nanospheres and nanothorn structures.[31–33] In our study, UL-AuNPs were synthesized via the chemical reaction of H_2O_2 using silver ions (Ag^+) for inducing nanothorn

structures. The reduction of gold nanoparticles to gold ions by H_2O_2 has been reported in several studies.[36,37] The anisotropic growth of gold nanothorns on the surface of UL-AuNPs was induced by adding a small amount of Ag^+.[31–33] The average size of UL-AuNPs was approximately 60–80 nm, and the maximum wavelength of absorption was 730 nm, as shown in Figure 2. UL-AuNPs can be easily dispersed in water-soluble PEDOT:PSS. However, UL-AuNPs did not blend well within the P3HT:PCBM active layer and were not substantially deposited onto the active layer.

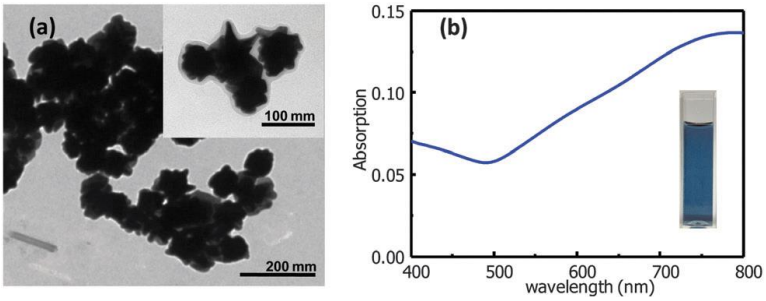

Figure 2. TEM image of (a) UL-AuNPs and (b) the UV-vis spectrum of 0.05mM UL-AuNPs in water. The scale bars indicate 200 nm and 100 nm.

When UL-AuNPs were blended with the P3HT:PCBM layer, a rough surface morphology was observed (Supporting information, Figure S3) which could result from the aggregation of UL-AuNPs in P3HT:PCBM, which is dissolved in an organic solvent. Hence, the performance of OSCs decreased when UL-AuNPs were blended with the active layer. These results are further highlighted in the Supporting information (Figure S4). We studied the effect of UL-AuNPs dispersed in PEDOT:PSS films. The UV-vis absorption of PEDOT:PSS films, after blending with UL-AuNPs, was measured at various concentrations of UL-AuNPs (Figure 3). The UV-vis spectrum shows that the absorption of PEDOT:PSS films is clearly dependent on the concentration of UL-AuNPs. The absorption of PEDOT:PSS films in the wavelength range 500–800 nm increased when PEDOT:PSS films were blended with UL-AuNPs. Moreover, the baseline spectrum of PEDOT:PSS films was shifted when UL-AuNPs

were incorporated into the PEDOT:PSS layer. The increase in absorption depends on the effect of UL-AuNP LSPR and Mie scattering.[13]

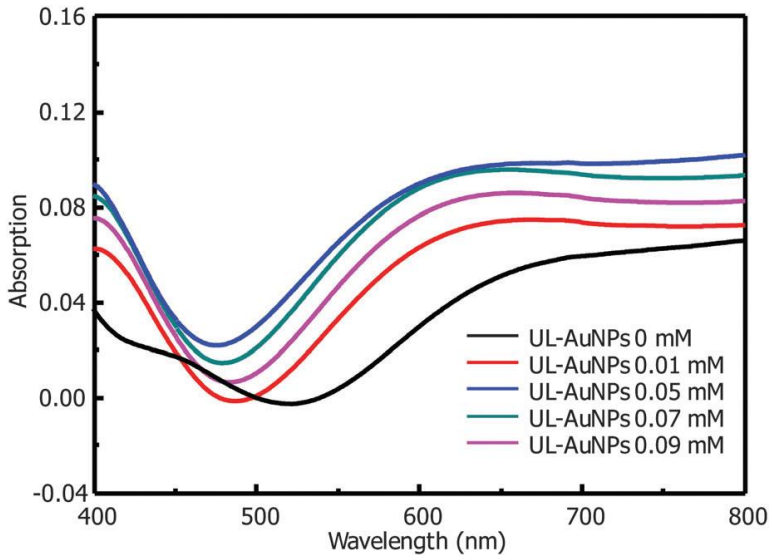

Figure 3. UV-vis spectra showing the effect of UL-AuNP concentration on the absorption of PEDOT:PSS films.

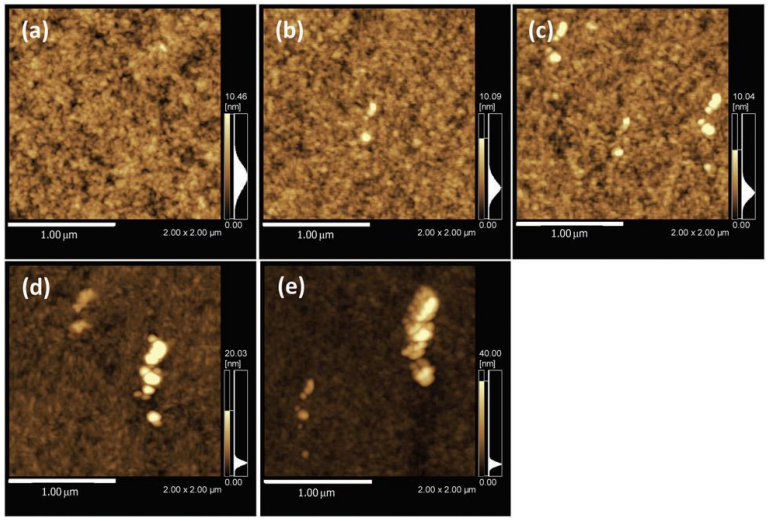

Figure 4. AFM images of PEDOT:PSS films after the addition of UL-AuNPs via a blending process. (a) 0 mM UL-AuNPs, (b) 0.01 mM UL-AuNPs, (c) 0.05 mM UL-AuNPs, (d) 0.07 mM UL-AuNPs, and (e) 0.09 mM UL-AuNPs.

However, when the concentration of UL-AuNPs was increased to 0.07 mM, absorption began to decrease, indicating that certain aspects of UL-AuNPs disappear from the film. To study this phenomenon, we evaluated the AFM images of the films (Figure 4). The AFM images reveal a smooth surface and the presence of a small amount of UL-AuNPs on the PEDOT:PSS film at both 0.01 mM and 0.05 mM, indicating that UL-AuNPs are well dispersed in the PEDOS:PSS films. However, when the concentration was increased to 0.07 mM, UL-AuNPs aggregate and clusters were observed on the PEDOT:PSS films. Typically, nanoparticles without a stabilizer or a capping agent tend to aggregate and precipitate to reduce the surface energy of the system.[38]

Effect of UL-AuNPs in OSCs

The current density versus voltage (*J–V*) properties and photovoltaic parameters of the fabricated OSCs, with and without UL-AuNPs in PEDOT:PSS films, are given in Figure 5 and Table 1, respectively. The standard deviation was obtained by measuring three different devices of the same structure. To study the effect of UL-AuNPs, the concentration of UL-AuNPs in the PEDOT:PSS films was increased from 0.01 mM to 0.09 mM. The reference cells without UL-AuNPs (UL-AuNPs at 0 mM) exhibit a short circuit current density (J_{SC}) of 6.2 ± 0.1 mA cm^{-2}, an open circuit voltage (V_{OC}) of 0.622 ± 0.005 V, a fill factor (FF) of 0.60 ± 0.01, and a solar cell efficiency (η %) of 3.07 ± 0.06%. The J_{SC} values of OSCs with 0.01 mM and 0.05 mM UL-AuNPs increased to 6.41 ± 0.08 mA cm^{-2} and 6.9 ± 0.1 mA cm^{-2}, respectively, in comparison to the reference cell. In contrast, V_{OC} was not significantly altered. The results indicate that the UL-AuNPs increased the number of photocarriers through increased light trapping at these concentrations but did not affect the energy diagram of P3HT:PCBM layers. Hence, an enhancement of approximately 12.21% in J_{SC} and approximately 5.86% in η was obtained in the case of 0.05 mM concentration. However,

OSCs with 0.07 mM and 0.09 mM UL-AuNPs exhibited a decrease in J_{SC} and η compared to the reference cell. Furthermore, with 0.09 mM UL-AuNPs, an obvious decrease in the V_{OC} and *J–V* curves was observed (Figure 5). This can be explained by the following reasons. (1) The large aggregation of UL-AuNPs in PEDOT:PSS films shown in the AFM image (Figure 4e) causes a connection between the anode and the active layer, resulting in a short circuit in the system. Indeed, a decrease of shunt resistance (R_{sh}), originating from the leak current, was observed at 0.09 mM UL-AuNPs (Supporting information, Figure S5). Although the reason for an increase of R_{sh} at 0.07 mM is not yet clear, this indicates that there is no current leakage at this concentration. (2) There is contact between the UL-AuNP aggregates in the PEDOT:PSS layer and P3HT:PCBM layers, which interferes with electron or hole transport. Such a contact is possible because gold aggregates can act as a recombination center.[39–41] To investigate the decay of η (%) with UL-AuNPs at high concentrations, we measured the interfacial properties of the OSCs by impedance spectroscopy.

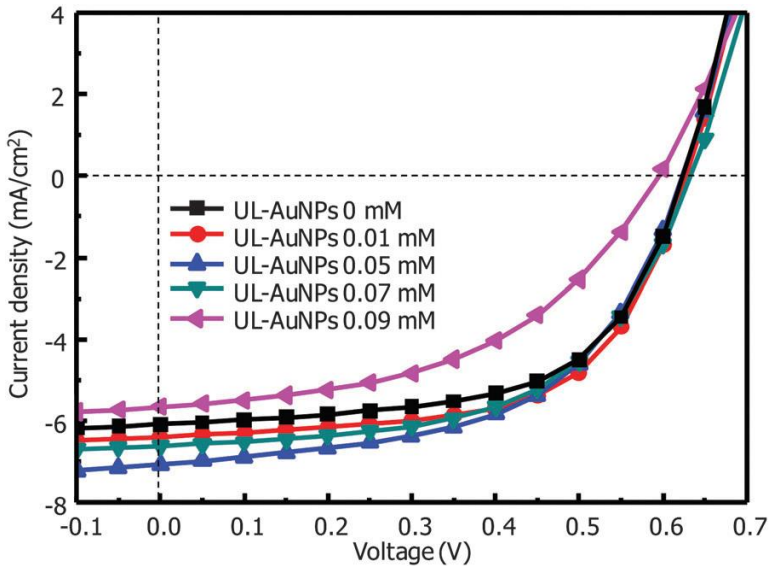

Figure 5 *J–V* properties of OSCs with UL-AuNPs in OSCs blended with PEDOT:PSS compared with reference cells.

Table 1. The photovoltaic parameters of OSCs with different conditions

	J_{sc} (mA/cm^2)	V_{oc} (V)	FF	η(%)
Reference cells	6.2±0.1	0.622±0.005	0.60±0.01	3.07±0.06
UL-AuNPs 0.01 mM	6.41±0.08	0.627±0.001	0.60±0.01	3.23±0.04
UL-AuNPs 0.05 mM	6.9±0.1	0.625±0.002	0.56±0.02	3.3±0.1
UL-AuNPs 0.07 mM	6.54±0.06	0.635±0.003	0.57±0.01	3.13±0.03
UL-AuNPs 0.09 mM	5.7±0.1	0.59±0.01	0.48±0.01	2.2±0.1

Impedance spectroscopy of OSCs

Impedance spectroscopy is a useful technique to investigate the interfacial properties of solar cells, such as electron transport and recombination.[42,43] To identify the difference in the interfacial properties of these photovoltaic cells, impedance spectra were acquired at an open-circuit voltage in the frequency range of 1 Hz to 1 MHz, an alternate current amplitude of 15 mV, and under solar light irradiation at 75 mW cm^{-2}.The Nyquist plots of the impedance spectra at various concentrations of UL-AuNPs in OSCs are shown in Figure 6. Single semicircular curves were observed at all concentrations. The Z´ value (approximately 9 Ω) on the left-hand side of the semicircle is equivalent to the series resistance of the circuit, which is similar to the values obtained from extrapolating *J–V* curves. The diameter of the semicircle at this frequency is related to the bulk resistance of the circuit.[44–46] As seen from the figure, the diameter of the semicircle decreases with increasing UL-AuNP concentration up to 0.05 mM, which also indicates a decrease in bulk resistance. This is reasonable because a small amount of metallic nanoparticles in the PEDOT:PSS film should decrease the resistance of the film.[47] However, when the concentration of the UL-AuNPs is increased to 0.07 mM the diameter of the semicircle tends to increase; moreover, at 0.09 mM, the diameter of the semicircle is greater than that of the reference OSCs without UL-AuNPs.

This indicates that the bulk resistance is higher than that of the reference OSCs. The observed trend correlates well with the efficiency η of OSCs.

To explore the effect of UL-AuNPs on the carrier transport and recombination in OSCs, the Bode phase plots were investigated (Supporting information, Figure S6). Generally, the single characteristic frequency peak (f_{max}) correlates with the photoinduced carrier lifetime (τ) in the nanocomposite electrodes, which relates to the efficiency of OSCs, as explained by the following equation:40,41

$$\tau = 1/(2\pi f_{max}) \qquad (1)$$

The probability of carrier recombination increases when the carrier lifetime decreases. The table inserted in Figure S6 in the supporting information shows that the carrier lifetime is slightly decreased by adding 0.01 and 0.05 mM UL-AuNPs, which could be due to an increase in the number of photocarriers, resulting in an increase in electron–hole recombination (Supporting information, Figure S6, inset table). This indicates that the increase in the number of photocarriers enhances the photocurrent even with an increase in recombination probability. Normally, AuNPs act as recombination centers and decrease the carrier lifetime of the device to some extent.[39,40] However, the lifetime of the electrons is then increased to a value similar to that of the reference cell (UL-AuNPs at 0 mM) by adding UL-AuNPs at concentrations of 0.07 and 0.09 mM. However, in this study, the lifetime (τ) at higher concentration is still not longer than that of the reference cell without UL-AuNPs. Therefore, the decreased efficiency of OSCs with 0.07 and 0.09 mM UL-AuNPs is probably not due to the increase in the number of recombination centers but due to the leak current originating from the large aggregation of UL-AuNPs.

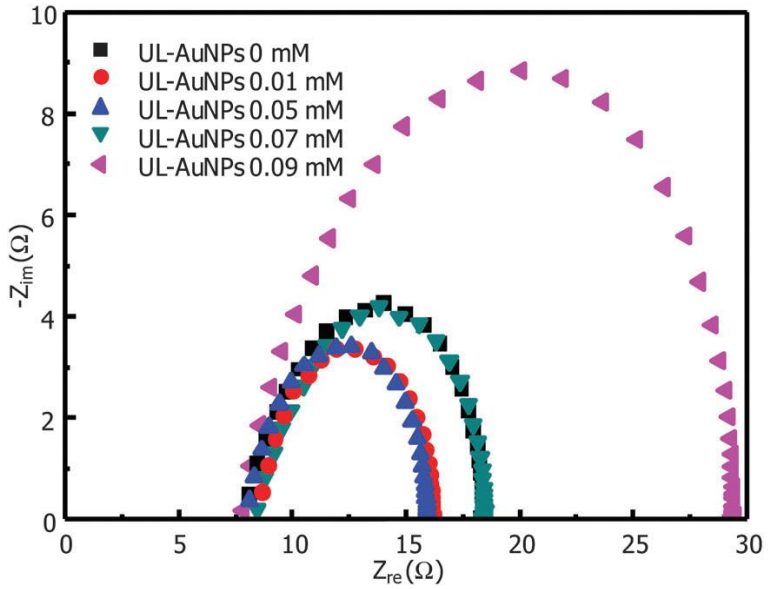

Figure 6 Nyquist plots of OSCs show the effect of UL-AuNP concentration on OSCs blended with PEDOT:PSS and a comparison with reference OSCs (UL-AuNPs at 0 mM).

Comparison of OSC properties with UL-AuNPs and with AuNPs

To further study the effect of nanothorn structures on UL-AuNPs, we compared the properties of OSCs with spherical AuNPs of the same size (Supporting information, Figure S7) and concentration (0.05 mM for both UL-AuNPs and spherical AuNPs). The incident photon-to-current efficiency (IPCE) of the fabricated OSCs is shown in Figure 7a. OSCs with both UL-AuNPs and AuNPs exhibited a higher IPCE as compared to the reference OSCs over a broad wavelength range. The increase in η for OSCs with UL-AuNPs and spherical AuNPs was approximately 6% and 3%, respectively, as compared to that of the reference cell (Supporting information, Figure S8). Furthermore, we observed that OSCs with UL-AuNPs exhibited a higher efficiency than those with spherical AuNPs. To conclusively show the effects of UL-AuNPs and spherical AuNPs, the enhancement factor (E.F.), which is the ratio of the IPCE of UL-AuNPs or spherical AuNPs to that of the reference OSCs without AuNPs, was determined (Figure 7b). UV-vis absorption spectra of UL-AuNPs and spherical AuNPs were also similarly compared to that of the reference OSCs (Figure 7b). In the case of OSCs

with spherical AuNPs, the IPCE was enhanced in the 400–620 nm range as compared to that of the reference OSCs. This is reasonable because the spherical AuNPs exhibit LSPR at approximately 500 nm to 600 nm.[47–50] In contrast, the IPCE of OSCs with UL-AuNPs was enhanced over a broad wavelength range because UL-AuNPs have a broad LSPR peak as compared to the spherical AuNPs of the same particle size (Figure 7b). At lower wavelengths (<500 nm), the enhanced IPCE could be attributed to the enhanced light scattering from the AuNPs because there is no LSPR peak in this wavelength region. Even in the 400–500 nm wavelength region, the IPCE of OSCs with UL-AuNPs was higher than that of OSCs with spherical AuNPs. This could be due to the large light scattering originating from the gold nanothorn structures on the particle surface.[31–33]

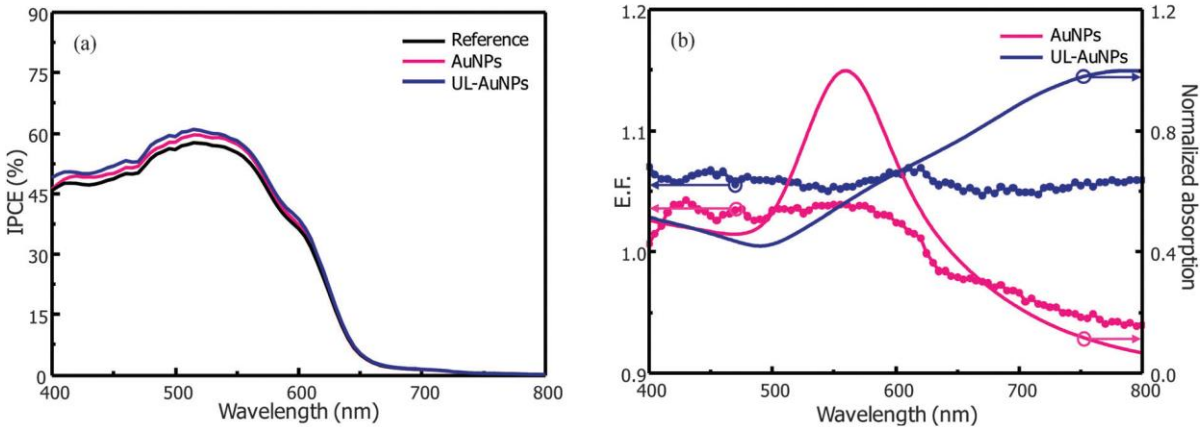

Figure 7 (a) Incident photon-to-current efficiency (IPCE) and (b) enhancement factor (E.F.) versus UV-vis spectra showing the effect of particle shape between AuNPs and UL-AuNPs on OSCs.

To evaluate the enhanced electric field from the nanothorn structures, FDTD simulations (FDTD solutions, Lumerical solutions, Inc. Canada) were performed. It has been reported that the increase in the electric field around the AuNPs corresponds to the enhancement of absorption and light scattering in the layer.[13]

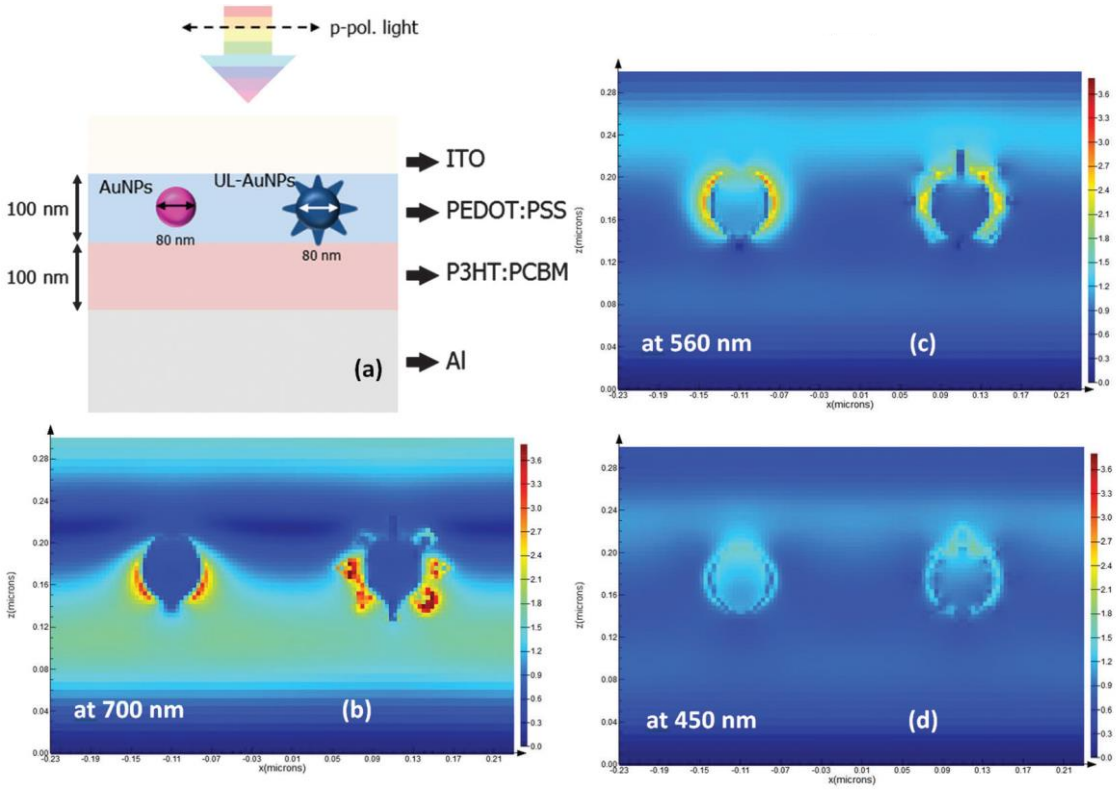

Figure 8 (a) Schematic of the simulated structure and electric field intensity map in OSCs with UL-AuNPs (right) and spherical AuNPs (left) at an irradiation wavelength of (b) 700 nm, (c) 560 nm, and (d) 450 nm.

As shown in Figure 8, UL-AuNPs show an enhanced electric field at 700 nm, located near each nanothorn. This result corresponds to the enhanced efficiency of OSCs in the longer wavelength region (Figure 7b). In the case of spherical AuNPs, the electric field enhancement is still observed at 700 nm. The reason for the decrease in the efficiency of OSCs in this wavelength region for spherical AuNPs remains unclear. However, the FDTD simulations indicate that the UL-AuNPs exhibited higher electric field enhancements in comparison to spherical AuNPs. At 560 nm, spherical AuNPs show a higher electric field enhancement in comparison to UL-AuNPs, corresponding to the LSPR absorption spectra shown in Figure 7b. At this wavelength, the IPCE of OSCs with UL-AuNPs is higher than that of OSCs with spherical AuNPs, although both OSCs were better than the reference OSCs. One possibility

for this is that each of the nanothorns enhances light scattering more than the spherical AuNPs. At 450 nm, the electric field intensity for both UL-AuNP and spherical AuNPs is slightly enhanced, which corresponds to the IPCE results. Hence, we believe that the improvement of OSCs with UL-AuNPs should be due to the plasmonic electric field enhancement/scattering effect.

CONCLUSIONS

In this study, we demonstrated the use of unique UL-AuNPs for OSC applications. UL-AuNPs in PEDOT:PSS films play an important role in improving the power conversion efficiency through an enhanced electric field and light scattering within OSCs. We observed that the efficiency of OSCs with UL-AuNPs was not only higher than that of a reference cell without nanoparticles but also higher than that of OSCs with spherical AuNPs. Furthermore, to understand the experimental results, FDTD simulations were performed by assuming the UL-AuNP structure in OSCs. FDTD simulations indicate an increased electric field distribution around gold nanothorns, which is in agreement with the experimental results. Based on our results, we conclude that the use of UL-AuNPs offers new opportunities toward a remarkable increase in the efficiency of OSCs.

REFERENCES

1. S. Lizin, S. Van Passel, E. De Schepper, W. Maes, L. Lutsen, J. Manca and D. Vanderzande, *Energy Environ. Sci.*, 2013, **6**,3136–3149.
2. C. V. Kumar, L. Cabau, A. Viterisi, S. Biswas, G. D. Sharma and E. Palomares, *J. Phys. Chem. C*, 2015, **119**, 20871–20879.
3. M. C. Scharber and N. S. Sariciftci, *Prog. Polym. Sci.*, 2013, **38**, 1929–1940.
4. T. M. Eggenhuisen, Y. Galagan, A. F. K. V. Biezemans, T. M. W. L. Slaats, W. P. Voorthuijzen, S. Kommeren, S. Shanmugam, J. P. Teunissen, A. Hadipour, W. J. H.

Verhees, S. C. Veenstra, M. J. J. Coenen, J. Gilot, R. Andriessen and W. A. Groen, *J. Mater. Chem. A*, 2015, **3**, 7255–7262.

5. Z. Tang, W. Tress and O. Ingana¨s, *Mater. Today*, 2014, **17**, 389–396.
6. T. Xu and L. Yu, *Mater. Today*, 2014, **17**, 11–15.
7. M. Koppe, H. J. Egelhaaf, G. Dennler, M. C. Scharber, C. J. Brabec, P. Schilinsky and C. N. Hoth, *Adv. Funct. Mater.*, 2010, **20**, 338–346.
8. Y. J. Cheng, S. H. Yang and C. S. Hsu, *Chem. Rev.*, 2009, **109**, 5868–5923.
9. J. Cai and L. Qi, *Mater. Horiz.*, 2015, **2**, 37–53.
10. J. N. Munday and H. A. Atwater, *Nano Lett.*, 2010, **11**, 2195–2201.
11. K.-S. Han, H. Lee, D. Kim and H. Lee, Sol. *Energy Mater. Sol. Cells*, 2009, **93**, 1214–1217.
12. M. Sharma, P. R. Pudasaini, F. Ruiz-Zepeda, D. Elam and A. A. Ayon, *ACS Appl. Mater. Interfaces*, 2014, **6**, 4356–4363.
13. H. A. Atwater and A. Polman, *Nat. Mater.*, 2010, **9**, 205–213.
14. A. Ng, W. K. Yiu, Y. Foo, Q. Shen, A. Bejaoui, Y. Zhao, H. C. Gokkaya, A. B. Djurisˇic´, J. A. Zapien, W. K. Chan and C. Surya, *ACS Appl. Mater. Interfaces*, 2014, **6**, 20676–20684.
15. L. Lu, Z. Luo, T. Xu and L. Yu, *Nano Lett.*, 2013, **13**, 59–64.
16. O. El Daif, L. Tong, B. Figeys, K. Van Nieuwenhuysen, A. Dmitriev, P. Van Dorpe, I. Gordon and F. Dross, Sol. *Energy Mater. Sol. Cells*, 2012, **104**, 58–63.
17. B. Cantaert, D. Ding, C. Rieu, L. Petrone, S. Hoon, K. H. Kock and A. Miserez, *Macromol. Rapid Commun.*, 2015, **36**, 1877–1883.
18. S. Vantasin, P. Pienpinijtham, K. Wongravee,C. Thammacharoen and S. Ekgasit, *Sens. Actuators, B*, 2013, **177**, 131–137.

19.L. Rodrı´guez-Lorenzo, R. de la Rica, R. A. A´lvarez-Puebla, L. M. Liz-Marza´n and M. M. Stevens, *Nat. Mater.*, 2012, **11**, 604–607.

20.C. C. Huang, Z. Yang, K. H. Lee and H. T. Chang, *Angew. Chem., Int. Ed.*, 2007, **46**, 6824–6828.

21.X. Li, W. C. H. Choy, L. Huo, F. Xie, W. E. I. Sha, B. Ding, X. Guo, Y. Li, J. Hou, J. You and Y. Yang, *Adv. Mater.*, 2012, **24**, 3046–3052.

22.M. Notarianni, K. Vernon, A. Chou, M. Aljada, J. Liu and N. Motta, *Sol. Energy*, 2014, **106**, 23–37.

23.J. Yang, J. You, C.-C. Chen, W.-C. Hsu, H.-r. Tan, X. W. Zhang, Z. Hong and Y. Yang, *ACS Nano*, 2011, **5**, 6210–6217.

24.P. R. Pudasaini and A. A. Ayon, *Phys. Status Solidi A*, 2012, **209**, 1475–1480.

25.X. Huang and M. A. El-Sayed, *J. Adv. Res.*, 2010, **1**, 13–28.

26.F. H. James, N. S. Daniel and M. S. Henry, *Phys. Med. Biol.*, 2004, **49**, N309.

27.D. A. Giljohann, D. S. Seferos, W. L. Daniel, M. D. Massich, P. C. Patel and C. A. Mirkin, *Angew. Chem., Int. Ed.*, 2010, **49**, 3280–3294.

28.S. Y. Khoo, H. Yang, Z. He, J. Miao, K. C. Leong, C. M. Li and T. T. Yang Tan, *J. Mater. Chem. A*, 2013, **1**, 5402–5409.

29.C. C. D. Wang, W. C. H. Choy, C. Duan, D. D. S. Fung, W. E. I. Sha, F.-X. Xie, F. Huang and Y. Cao, *J. Mater. Chem.*, 2012, **22**, 1206–1211.

30.C. Fei Guo, T. Sun, F. Cao, Q. Liu and Z. Ren, *Light: Sci. Appl.*, 2014, **3**, e161.

31.H. Yuan, C. G. Khoury, H. Hwang, C. M. Wilson, G. A. Grant and T. Vo-Dinh, *Nanotechnology*, 2012, **23**, 075102.

32.H. Yuan, W. Ma, C. Chen, J. Zhao, J. Liu, H. Zhu and X. Gao, *Chem. Mater.*, 2007, **19**, 1592–1600.

33.H. Yuan, W. Ma, C. Chen, H. Zhu, X. Gao and J. Zhao, *J. Mater. Chem. C*, 2011, **115**, 23256–23260.

34.D. Kozanoglu, D. H. Apaydin, A. Cirpan and E. N. Esenturk, *Org. Electron.*, 2013, **14**, 1720–1727.

35.M. Sharma, P. R. Pudasaini, F. Ruiz-Zepeda, E. Vinogradova and A. A. Ayon, *ACS Appl. Mater. Interfaces,* 2014, **6**, 15472–15479.

36.S. Nootchanat, C. Thammacharoen, B. Lohwongwatana and S. Ekgasit, *RSC Adv.*, 2013, **3**, 3707–3716.

37.Q. Li, B. Lu, L. Zhang and C. Lu, *J. Mater. Chem.*, 2012, **22**, 13564–13570.

38.Y. Xia, Y. Xiong, B. Lim and S. E. Skrabalak, *Angew. Chem., Int. Ed.*, 2009, **48**, 60–103.

39.L. Faraone, A. G. Nassibian and J. G. Simmons, *J. Appl. Phys.*, 1978, **49**, 6185–6186.

40.S. Nootchanat, H. Ninsonti, A. Baba, S. Ekgasit, C. Thammacharoen, K. Shinbo, K. Kato and F. Kaneko, *Phys. Chem. Chem. Phys.*, 2014, **16**, 24484–24492.

41.J. Feng, Y. Hong, J. Zhang, P. Wang, Z. Hu, Q. Wang, L. Han and Y. Zhu, *J. Mater. Chem. A*, 2014, **2**, 1502–1508.

42.S. Nho, G. Baek, S. Park, B. R. Lee, M. J. Cha, D. C. Lim, J. H. Seo, S.-H. Oh, M. H. Song and S. Cho, *Energy Environ. Sci.*, 2016, **9**, 240–246.

43.T. W. Zeng, I. S. Liu, F. C. Hsu, K. T. Huang, H. C. Liao and W. F. Su, *Opt. Express*, 2010, **18**, A357–A365.

44.B. J. Leever, C. A. Bailey, T. J. Marks, M. C. Hersam and M. F. Durstock, *Adv. Energy Mater.*, 2012, **2**, 120–128.

45.G. Perrier, R. de Bettignies, S. Berson, N. Lemaıˆtre and S. Guillerez, *Sol. Energy Mater. Sol. Cells*, 2012, **101**, 210–216.

46.G. Garcia-Belmonte, A. Munar, E. M. Barea, J. Bisquert, I. Ugarte and R. Pacios, *Org. Electron.*, 2008, **9**, 847–851.

47. C. E. Cheng, Z. Pei, C. C. Hsu, C. S. Chang and F. Shih-Sen Chien, *Sol. Energy Mater. Sol. Cells*, 2014, **121**, 80–84.

48. G. D. Spyropoulos, M. M. Stylianakis, E. Stratakis and E. Kymakis, *Appl. Phys. Lett.*, 2012, **100**, 213904.

49. D. D. S. Fung, L. Qiao, W. C. H. Choy, C. Wang, W. E. I. Sha, F. Xie and S. He, *J. Mater. Chem.*, 2011, **21**, 16349–16356.

50. G. Chen, J. Seo, C. Yang and P. N. Prasad, *Chem. Soc. Rev.*, 2013, **42**, 8304–8338.

CHAPTER III

Investigation of Gold Quantum Dots Enhanced Organic Thin Film Solar Cells

ABSTRACT

In this study, the effect of gold quantum dots (AuQDs) on organic thin-film solar cells (OSCs) are demonstrated to improve their photoelectric conversion properties. Three types of AuQDs with different fluorescence emission wavelengths: blue (B-AuQDs); green (G-AuQDs); and red (R-AuQDs) are used. The emission wavelengths depended on the number of gold atoms within the AuQDs. AuQDs were loaded into a poly(3,4-ethylenedioxythiophene):poly(styrene sulfonate) thin-film layer of OSCs. UV–vis spectra, atomic force microscope images, current density versus voltage properties, and the impedance spectra of the fabricated devices were measured for the aforementioned three types of AuQDs. The AuQDs were able to act as a photosensitizer to improve short-circuit current of OSCs. An efficiency increase of 10% with G-AuQDs-loaded OSCs was obtained compared to OSCs without the AuQDs. The fluorescence of the AuQDs played an important role in the enhancement of the OSCs. Finite-difference time-domain simulations indicated that electric field distributions depended on the degree of aggregation within the AuQDs.

INTRODUCTION

There has been a great deal of interest in applying light-harvesting systems that use gold quantum dots (AuQDs) because their size enables them to offer both distinctive functionalities and the ability to exhibit fluorescence in the visible range.[1,2] When the diameter of gold becomes less than 2 nm, they are called AuQDs (or gold nanoclusters) and exhibit quantum effect instead of plasmonic effect. This means that the number of gold atoms in the AuQDs determines the wavelength of the fluorescence emission due to the quantum effect. Electrons in AuQDs are excited from the ground state to the excited state by absorbing mainly near-UV light.[3,4] This implies that AuQDs can harvest light from the UV region and convert it into visible light. Because most organic photoelectric-converting materials

harvest light mostly in the visible range, one important challenge is to apply AuQDs especially in organic light-harvesting systems.

The use of AuQDs for photoelectric conversion systems was first reported on by Tatsuma *et al*.[5,6] In their work, AuQDs were used as photosensitizers on TiO_2 electrodes that were used for light-harvesting in the visible to near-infrared region. Furthermore, AuQDs have been used to improve dye-sensitized solar cells.[7,8] In these studies, AuQDs were used to enlarge the harvesting wavelength as well as the absorption region of the dyes.

Organic thin-film solar cells (OSCs) are one of the most promising candidates for inexpensive and flexible photovoltaic cells based on organic materials.[9-12] Gold nanoparticles (AuNPs), which is bigger than AuQDs and typically have a diameter from 2 to 100 nm, exhibit strongly enhanced localized electric field due to the plasmonic effect and have also shown promise in this field as various studies have reported on improvements of OSCs using AuNPs.[13,14] Due to the excitation of localized surface plasmon resonance (LSPR) and light scattering known as Mie scattering,[15,16] strong light absorption can be obtained in OSCs with AuNPs.[17,18] In these studies, AuNPs were used, for example, by blending them into the active layer [19,20] and hole transport layer.[21,22] We have also reported on how the performance of OSCs can be enhanced using metal nanoparticles, such as spherical AuNPs and urchin-like AuNPs.[23]

Another approach to enhancing OSCs has been through the use of semiconductor QDs [24,25] and graphene QDs.[26] For example, Li *et al.* reported that blending $CuInS_2$/ZnS-QDs in the active layer of OSCs improved the photocurrent in the visible range; the materials absorbed and emitted UV and visible light, respectively, due to the quantum effect of the semiconductor QDs.[22] Another semiconductor QD was also used to improve the photocurrent; it did this by enabling charge transport from the PbS QDs to the active layer.[27]

In this study, we investigate the effect of AuQDs on OSCs in order to improve their photoelectric conversion properties. To the best of our knowledge, this is the first report of the use of AuQDs in OSCs. Emissions from blue (B-AuQDs), green (G-AuQDs), and red (R-AuQDs) gold quantum dots were investigated for light-harvesting in the near-UV region. UV–vis spectra, atomic force microscope (AFM) images, current density versus voltage (J–V) properties, and the impedance spectra of fabricated devices were measured with these three types of AuQDs. Our results demonstrate that all of these types of AuQDs, which had been loaded into a poly(3,4-ethylenedioxythiophene):poly(styrene sulfonate) (PEDOT:PSS) layer in OSCs, improved the power conversion efficiency of the OSCs by increasing the amount of photocarriers; notably, a 10% increase in the power conversion efficiency over that of reference cells was achieved through the use of G-AuQDs-loaded OSCs. We found that the fluorescence and aggregation of the AuQDs resulted in the plasmonic effect playing an important role in the enhancement of the OSCs. To further understand this effect, finite-difference time domain (FDTD) simulations were performed by assuming the AuQD and AuNP structures in the OSCs.

EXPERIMENTAL SECTION

Fabrication of AuQDs-loaded OSCs

Three types of AuQDs, B-AuQDs (mixture of Au_5 and Au_8 (5 and 8 Au atoms)), G-AuQDs (Au_{13} (13 Au atoms)), and R-AuQDs (Au_{25} (25 Au atoms)) were purchased from Dai Nippon Toryo Co. Ltd. To fabricate the AuQDs-loaded OSCs, AuQDs with different emission wavelengths, B-, G-, and R-AuQDs were loaded into the PEDOT:PSS (Clevios, Heraeus Co.) layer of OSCs. The AuQDs were diluted to a concentration of 0–4.00 μM in deionized water. Each AuQDs solution was mixed with PEDOT: PSS (1:6 v/v) and sonicated for 1 h. The AuQDs-loaded PEDOT:PSS layers, which each had a thickness of ~100 nm (supporting

information, Figure S5) were deposited onto ITO substrates (FINE brand, Furuuchi Co. Ltd, 10 Ω cm^{-2}) by spin-coating at 1000 rpm. Then, the PEDOT:PSS layers were annealed at 120 °C for 20 min.Phenyl-C61-butyric acid methyl ester (PCBM) and poly(3-hexylthiophene) (P3HT) (Sigma-Aldrich) were mixed in dichlorobenzene with a mass ratio of 1:0.8 and were deposited into the PEDOT:PSS layer by spin-coating at 1500 rpm, followed by annealing at 120 °C for 10 min. The thickness of the P3HT:PCBM layer was approximately 100 nm (Supporting information, Figure S6). A 150 nm thick aluminum back electrode was formed on the P3HT:PCBM layer *via* thermal evaporation. The fabricated AuQDs-loaded OSCs were annealed at 150 °C for 45 min in a vacuum chamber before further characterization.

Characterization

The UV–vis absorption spectra of the AuQDs solution, PEDOT:PSS films, and AuQDs-loaded PEDOT:PSS films were characterized by a UV–vis spectrometer (V-650, Jasco). The fluorescence spectra of AuQDs dispersions were monitored by a portable UV–vis–NIR spectrometer (SILVER-Nova 25, Stellar Net). The surface morphologies of the AuQDs-loaded PEDOT:PSS films were investigated using an AFM (SPM-9600, Shimadzu). The photovoltaic properties and impedance spectra of the fabricated OSCs were measured by a precision source-meter unit (B2901A, Agilent) and a potentiostat (PARSTAT 4000, Princeton Applied Research), respectively, under the irradiation of a solar simulator (HAL-C100, 100 W compact xenon light source, Asahi Spectra).

RESULTS AND DISCUSSION

Optical and AFM Properties of AuQDs-loaded PEDOT:PSS Films

In this study, we used three types of AuQDs: B-AuQDs (mixture of Au_5 and Au_8 (5 and 8 Au atoms)); G-AuQDs (Au_{13} (13 Au atoms)); and R-AuQDs (Au_{25} (25 Au atoms)). Figure 1

shows the UV–vis absorption and fluorescence spectra of these AuQDs. As shown in this figure, all of the AuQDs exhibit absorption at wavelengths lower than 500 nm, while there is very weak absorption in the visible light range. When the solutions were illuminated with UV light (365 nm), the B-, G-, and R-AuQDs emitted visible light with maximum emission peaks of 507, 520, and 650 nm, respectively (the photograph of the emission is seen in the inset). When illuminated by UV light, electrons in the ground state were excited and then relaxation took place, which allowed for the emission of visible light (fluorescence); this is attributed to the quantum size effect, which directly depends on the number of Au atoms in an AuQDs.[1,2] A lower number of Au atoms in a AuQD results in its emission peaks being blue-shifted. This phenomenon implies that AuQDs can act as a visible light generator. Thus, loading AuQDs into OSCs may enhance how much light is absorbed from solar light, because the incident photon-to-current efficiency (IPCE) of OSCs is usually much lower in the UV region than in the visible range region.

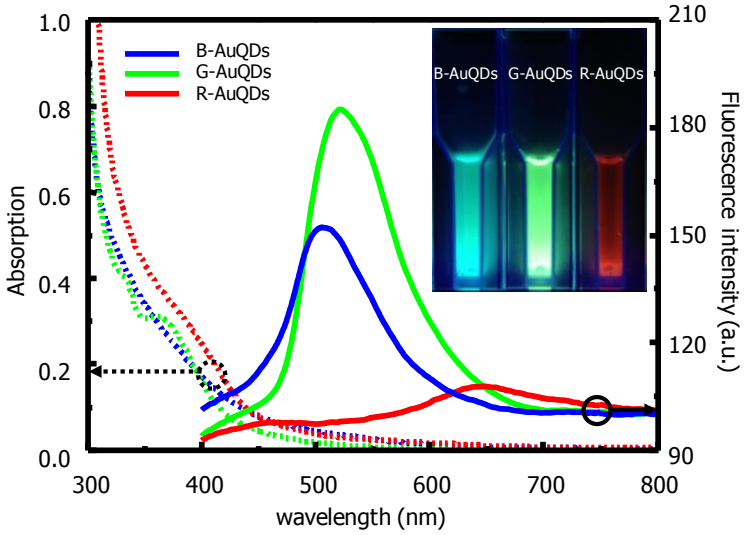

Figure 1. UV–vis absorption and fluorescence spectra of B- (0.01 mM), G-, (0.01 mM), and R-AuQDs (1.5 mM). The photographs show fluorescence of water-dispersed AuQDs under UV light (365 nm) illumination (inset).

Because both AuQDs and PEDOT:PSS are water-soluble, we loaded the AuQDs into the PEDOT:PSS layers. Figure 2 shows the UV–vis spectra of AuQD-loaded PEDOT:PSS films. The results show the absorption of PEDOT:PSS in two regions: in the range of 300–460 nm; and 460–900 nm. Higher absorption was observed in AuQDs-loaded PEDOT:PSS films at wavelengths of 300–400 nm than in the PEDOT:PSS film without AuQDs, which indicated that more UV light can be absorbed by the AuQDs. However, absorption above 500 nm decreased. One reason for this decrease might be due to the dilution of the PEDOT:PSS by adding water-soluble AuQDs. However, the decrease observed with R-AuQDs and G-AuQDs is more pronounced than it is with B-AuQDs. This implies that it may be due to the fluorescence of the AuQDs, which decrease the absorption intensity in longer wavelength regions of the AuQDs-loaded PEDOT:PSS films. This is a reasonable assumption to make because G-AuQDs emissions are both of a longer wavelength and stronger than those of B-AuQDs. Although R-AuQDs exhibit weak emission, their fluorescence wavelength is in the 550–800 nm range, which should cause a decrease in the absorption spectrum in the longer wavelength.

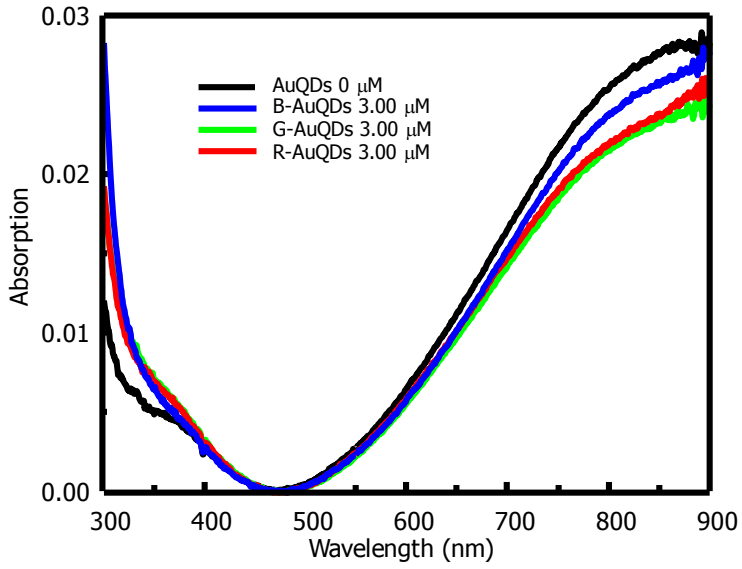

Figure 2. UV–vis spectra of AuQD-loaded PEDOT:PSS films cast onto glass substrates.

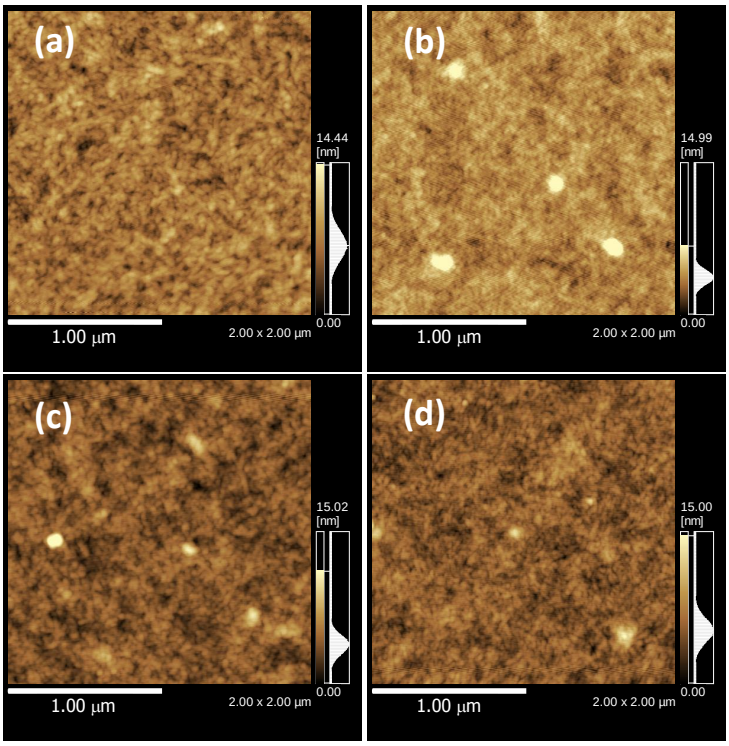

Figure 3. AFM images of (a) the PEDOT:PSS film, (b) 3.00 μM of the B-, (c) 3.00 μM of the G-, and (d) 3.00 μM of the R-AuQDs-loaded PEDOT:PSS film.

The effect of loading AuQDs onto the PEDOT:PSS layers on the morphologies was studied through AFM measurements, as shown in Figure 3. The AFM image reveals the smooth surface of the PEDOT:PSS film that did not contain AuQDs. For the PEDOT:PSS films with AuQDs, small islands were observed; these are attributable to the aggregation of AuQDs (Figure 3b–d); a large aggregation was observed in particular for the B-AuQDs-loaded PEDOT:PSS film. Usually, in the case of AuNPs, small nanoparticles have high surface energy due to their high surface area, and they tend to aggregate with adjacent particles in order to reduce their surface energy. The aggregation of the nanoparticles depends on their size and on their surrounding environment.[28] In our case, the B-AuQDs formed smaller clusters than G- and R-AuQDs. The smaller size of the B-AuQDs tended to result in a large aggregation of particles and create large islands on the surface of the PEDOT:PSS film. When the cluster size of the AuQDs increased (*i.e.*, B-AuQDs were the smallest, G-AuQDs

were larger, and R-AuQDs were the largest), the degree of aggregation gradually decreased. It should be noted that large aggregated-AuQDs cause the decrease of the AuQDs' fluorescence, which might affect its UV–vis spectra, as seen in Figure 2.

Impedance Spectroscopy of OSCs

To study the differences in interfacial properties of the OSCs with AuQDs, impedance spectra were measured. The Nyquist plots of the impedance spectra of the AuQDs-loaded OSCs, and OSCs without the AuQDs, under solar light illumination are shown in Figure 4b. The schematic of the fabricated OSCs is shown in Figure 4a. Because single semi-circle curves were observed in all cases, we assume a simple circuit model as shown in the inset. In this model, the R_s circuit element represents resistive losses in the ITO and PEDOT:PSS or PEDOT:PSS-AuQDs. This value corresponds to the intersection of the semicircles.[29] The R_s value of the AuQDs-loaded OSCs is slightly smaller than those of the OSCs without AuQDs, which indicates that the resistance of the PEDOT:PSS layer was decreased by it being loaded with AuQDs. The phase constant element (CPE) in parallel with the R_{ct} is used to explain a distribution of relaxation time at interfaces and nearly same as the differential capacitance.[29] The R_{ct} value represents the bulk resistance of P3HT:PCBM,[29-31] which decreased in the following order: OSCs without AuQDs (10.5 Ω); OSCs with B-AuQDs (10.3 Ω); with G-AuQDs (9.7 Ω); and with R-AuQDs (9.5 Ω). The decrease of R_{ct} is attributed to the increase in the number of charge carriers in the P3HT:PCBM layers. This indicates that the AuQDs, especially the G-AuQDs, generated more photocarriers in the P3HT:PCBM layer. Because the AuQDs are not included in the P3HT:PCBM active layer, one reason for the increase in the number of photocarriers is the increased visible light illumination due to fluorescence from the AuQDs along with the illuminated solar light. In addition to this effect, excited electrons adjacent to the P3HT:PCBM layer are injected to the

conduction band of PCBM layer. In fact, the R_{ct} values further decreased when the AuQDs were directly deposited on the PEDOT:PSS layer instead of mixing with the PEDOT:PSS. A schematic illustration of a proposed photocurrent generation mechanism is shown Figure 5.

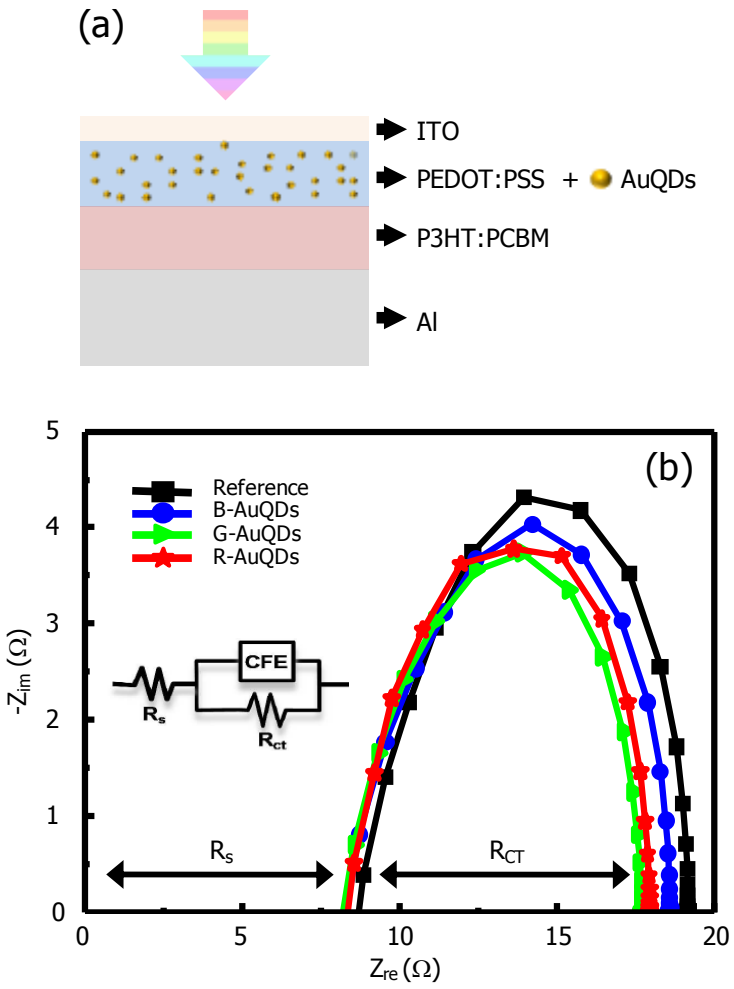

Figure 4. (a) Schematic of the fabricated AuQDs-loaded OSCs and (b) the Nyquist plots of the OSCs without AuQDs and the AuQDs-loaded OSCs under solar light illumination.

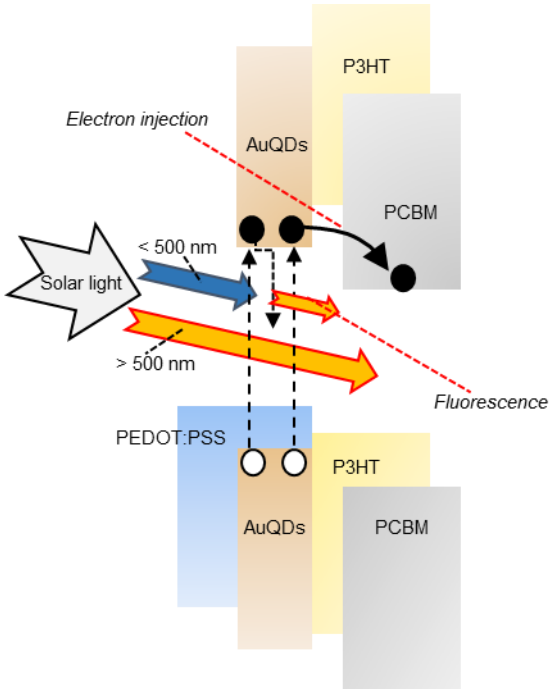

Figure 5. Schematic illustration of proposed AuQDs-induced photocurrent generation mechanism

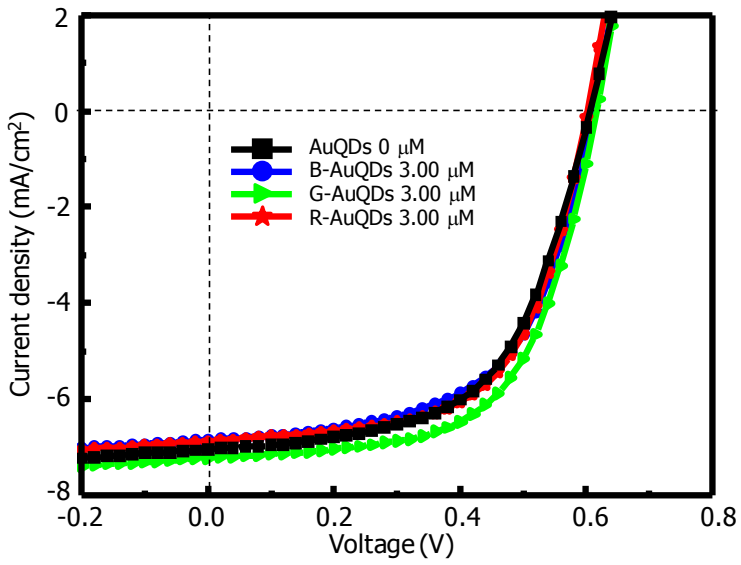

Figure 6. *J–V* property of the AuQDs-loaded OSCs compared with the reference OSCs.

Table 1. The photovoltaic parameters of OSCs with three types of AuQDs at 3.00 μM, and one reference OSC without any AuQDs.

	J_{SC} (mA/cm^2)	V_{OC} (V)	FF	η (%)
Reference OSCs	6.80	0.60	0.59	3.25
B-AuQDs-loaded OSCs	6.86	0.61	0.59	3.26
G-AuQDs-loaded OSCs	7.20	0.62	0.60	3.59
R-AuQDs-loaded OSCs	6.86	0.61	0.60	3.35

Photovoltaic Properties of AuQDs-loaded OSCs.

The current density versus voltage (*J–V*) properties and photovoltaic parameters (mean value) of both AuQDs-loaded OSCs (3.00 μM AuQDs) and reference OSCs (without AuQDs) are given in Figure 6 and Table 1, respectively. The photovoltaic properties of other conditions are also shown in Figure S3 and Table S1 (supporting information). The reference cells, which did not have AuQDs, exhibited a short-circuit current density (J_{SC}) of 6.80 mA/cm^2, an open circuit voltage (V_{OC}) of 0.60 V, a fill factor (FF) of 0.59, and a solar cell efficiency (η%) of 3.25%. The J_{SC} values of OSCs with B- and R-AuQDs increased to 6.86 mA, and the J_{SC} value of OSCs with G-AuQDs increased to 7.20 mA, which is about 5.9% greater than that of the reference OSCs. The value of the efficiency with G-AuQDs at 3.00 μM was also 10 % greater than that of the reference OSCs. The results corresponded with the impedance measurements, which showed the lowest impedance for the G-AuQDs-loaded OSCs. In contrast, V_{OC} for all OSCs did not change significantly. The results indicate that loading the AuQDs into the PEDOT:PSS layer increased the number of photocarriers. To study the effect of the AuQDs, we varied the concentration of the AuQDs in PEDOT:PSS from 1.00–4.00 μM as shown in Figure 7. The highest efficiency η was obtained with the 3.00 μM G- and R-AuQDs-loaded OSCs. The efficiency gradually increased as the

concentration increased up to 3.00 μM before it started decreasing at higher concentrations. In the case of the B-AuQDs, the efficiency gradually decreased from 1.00 μM. As observed in the AFM images, a large aggregation of AuQDs was observed in the B-AuQDs-loaded OSCs. Hence, the decrease in the efficiency was likely due to this large aggregation.

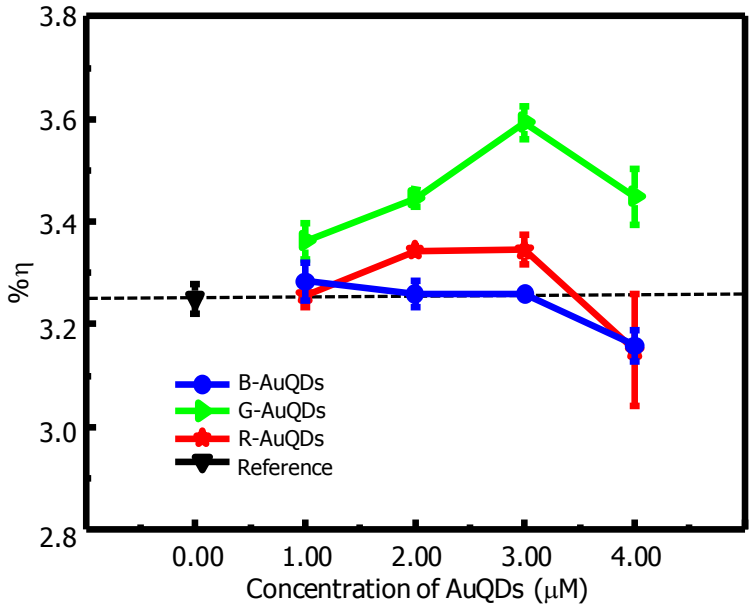

Figure 7. A summary of the solar cell efficiency ($\%\eta$) of the AuQDs-loaded OSCs as a function of concentration, with the reference OSCs provided as a comparison.

To further study the effect of AuQDs in the OSCs, we measured their IPCE, as shown in Figure 8(a). All the OSCs with AuQDs exhibited higher IPCE values in the broad wavelength range than the reference OSCs did. Again, the IPCE of the G-AuQD-loaded OSCs showed greater improvement than the R- and B-AuQDs-loaded OSCs did in a wide wavelength range. In order to show how the photocurrent was changed by loading the OSCs with AuQDs, we plotted the enhancement factor, which is the ratio of the IPCE values of AuQDs-loaded OSCs to that of the reference OSC, as shown in Figure 8 (b). We will break down our explanation of the results into two wavelength regions: 300–500 nm; and 500–800 nm. In the 300–500 nm region, the AuQDs exhibited absorption, meaning that incident light can be converted

into light of longer wavelengths by the fluorescence of the AuQDs, in addition to the electron injection to the PCBM layer from the excited state of the AuQDs as schematically shown in Figure 5. The enhancement factor was seen to increase at around 350 and 430 nm, where the AuQDs showed strong fluorescence at these excited wavelengths. This means that the number of photocarriers in the P3HT:PCBM layer can be increased when the AuQDs-loaded OSCs are illuminated by the light wavelength shorter than 500 nm. The enhancement factor was greater for the G-AuQDs than for the R-AuQDs and B-AuQDs when the same concentrations were used. This was because the fluorescence wavelength of the G-AuQDs was strongest, and it was the closest to the wavelength of the P3HT:PCBM absorption peak. R-AuQDs exhibited an enhancement factor that was greater than that of the B-AuQDs, though the R-AuQDs showed a lower fluorescence intensity than that of the B-AuQDs (Figure 1). The results corresponded with the results of the impedance measurements and AFM observations. (Figures 3 and 4). The small cluster size of the B-AuQDs exhibited large aggregations, which decreased the fluorescence and reduced the charge transport at the P3HT:PCBM/PEDOT:PSS interface, which resulted in the low enhancement factor of the photocurrent.

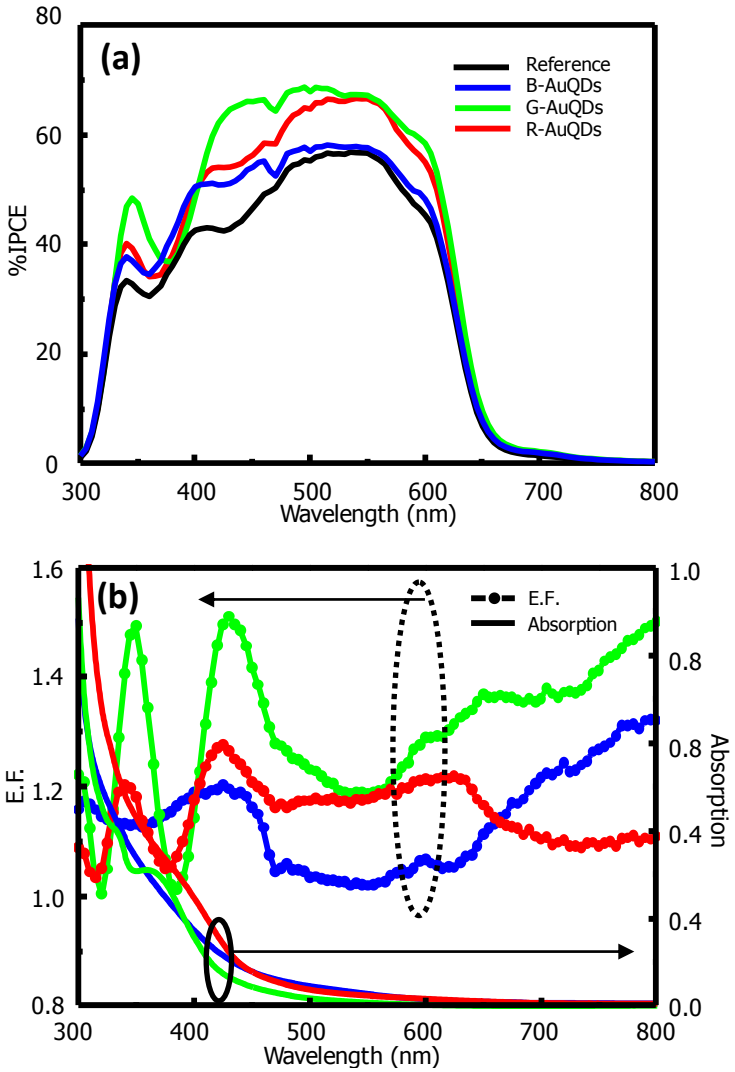

Figure 8. (a) Incident photon-to-current efficiency (IPCE) and (b) enhancement factor (E.F.) showing the effect of the variation of the AuQDs on the OSCs and corresponding absorption.

Secondly, in the longer wavelength region, *i.e.*, 500–800 nm, the AuQDs did not exhibit the absorption that had been observed in Figure 1; as a result, almost no fluorescence was observed. However, an increase in the enhancement factor was observed in this region. The B-AuQDs showed a stronger enhancement than the R-AuQDs did for wavelengths longer than 670 nm. This might be explained by the small degree of the aggregation of the B-AuQDs, because the smaller AuQDs tend to aggregate more easily. It is known that the small particles reduce the surface energy, which induces them to form larger particles.[32]

Therefore, increasing the ionic strength of the PEDOT:PSS solution and mixing it in an ultrasonic bath might stimulate AuQDs aggregation in the system. According to the AFM images (Figure 3), a large aggregation of AuQDs is visible in the 30–200 nm for all of the AuQDs types. This large aggregation caused a decrease in the IPCE, as explained in the previous section. However, it is reasonable to consider that the smaller aggregation in the 5–20 nm range was formed as alongside the larger aggregates. The size of the gold particles became greater than 2 nm due to these aggregations, *i.e.*, AuNPs were formed, and as a result the quantum effect did not appear; instead, localized surface plasmons could be excited as schematically shown in Figure 9. These localized surface plasmons could enhance the photoelectric current in the visible range by enhancing both the electric field and light scattering.[33] G-AuQDs also showed greater photocurrent in longer wavelength regions. In the case of the R-AuQDs, the increase in the photocurrent gradually decreased when the wavelength exceeded 630 nm. This means that G- and B-AuQDs were more affected by the localized surface plasmon effect than the R-AuQDs were. Furthermore, in this region, the enhancement factor might be more affected by the localized surface plasmons than by the fluorescence because the fluorescence of the R-AuQDs was not strong enough. It should be noted that the contribution of increased IPCE in the longer wavelength region (> 630 nm) to J_{sc} is much smaller than that in the shorter wavelength (< 630 nm) because of the absorption peak of P3HT:PCBM is at around 550 nm. Hence the increase of J_{sc} values with B-AuQDs is smaller than that with G- and R-AuQDs OSCs.

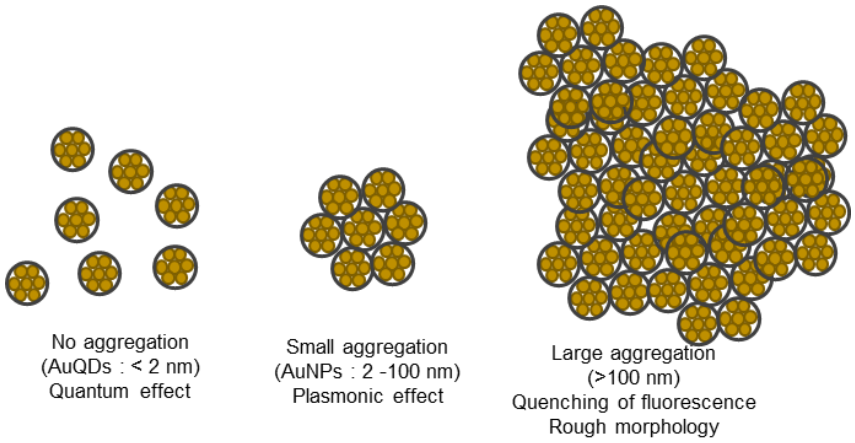

Figure 9. Schematic drawing of the aggregation of AuQDs

FDTD Simulations

To further explore the effect of the AuQDs, we studied the electric field enhancement using FDTD simulations; we did this by modeling the AuQDs and AuNPs in the PEDOT:PSS layer. As schematically outlined in Figure 10a, AuNPs with diameters of 20 and 5 nm, and AuQDs with diameters of 1.5 and 1 nm, were added into the PEDOT:PSS layer. The simulated results, under illumination of light at 350 nm, 550 nm, and 700 nm, are shown in Figure 10b–d. FDTD simulations of OSCs containing neither AuQDs nor AuNPs, OSCs with only AuQDs, and OSCs with only AuNPs, were also carried out; the results are shown in Figure S2-S4 (supporting information). The simulations clearly show that the AuQDs do not increase the electric field inside the OSCs, while the AuNPs enhance the electric field around the particles due to the excitation of localized surface plasmons. Therefore, the enhanced photocurrent below 500 nm is not due to the electric field enhancement of AuQDs. Since the IPCE peak was matched with the fluorescence excitation wavelength, increase of the photocurrent in this region should be affected by fluorescence of the AuQDs. Besides the fluorescence effect, the enhanced baseline of photocurrent might be due to some localized surface plasmons caused by the small degree of aggregation of the AuQDs. Furthermore, the

FDTD simulation exhibits that the localized surface plasmons enhance the electric field, especially at the side of P3HT:PCBM layer at 700 nm of illuminated light.

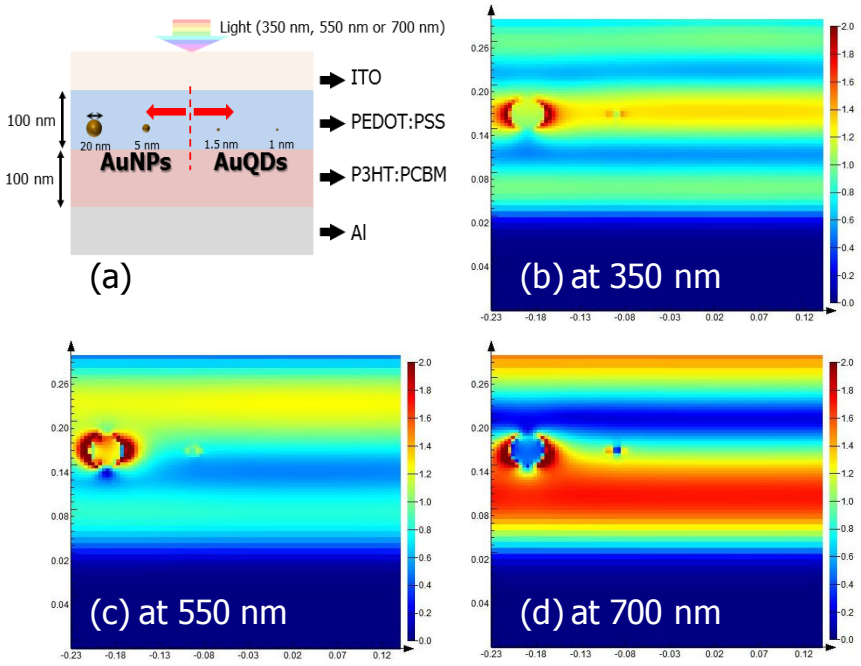

Figure 10. (a) Schematic of the simulated structure and electric field intensity map of the OSCs with AuNPs (diameter of 20 and 5 nm) and AuQDs (diameter of 1.5 and 1 nm) in the PEDOT:PSS layer at illumination wavelengths of (b) 350 nm, (c) 550 nm, and (d) 700 nm.

This simulation supports the IPCE results, which suggested that the small degree of aggregation of the AuQDs enhanced the photocurrent, especially at longer wavelengths. Therefore, we conclude that our developed AuQDs-loaded OSCs were mainly improved by both the fluorescence of AuQDs below 500 nm and plasmonic properties due to the small degree of AuQDs aggregation at longer wavelengths.

CONCLUSION

We demonstrated that using AuQDs in OSCs improves the performance of photovoltaic devices. We found that the AuQDs in the OSCs exhibit fluorescence, *i.e.*, conversion of the wavelength from shorter to longer wavelengths. This is useful for when the active layer has a region of low IPCE such as in the UV region; photon of that wavelength can then be converted into longer wavelength photons via the AuQDs for absorption by the active layer, which generally has a higher absorption coefficient at longer wavelengths. We studied three types of AuQDs; B-, G, and R-AuQDs. All of them improved solar cell efficiency, and the G-AuQDs exhibited the best improvement; this was because the fluorescent wavelength of the G-AuQDs matched the absorption wavelength of the active layer. Furthermore, we found that the aggregates of the Au-QDs played an important role, as they may aggregate enough to become AuNPs and so demonstrate localized surface plasmons, which may enhance the electric field or increase light scattering. By combining the fluorescence from the AuQDs and the small degree of aggregation of the AuQDs, an improvement in the photocurrent was obtained for a wide range of wavelengths. We further investigated our results through FDTD simulations; these were performed by making assumptions about the structure of the AuQDs and AuNPs in the OSCs. Our FDTD simulations indicated an increased electric field distribution that depended on the degree of aggregation of the AuQDs, which was in agreement with the experimental results. Based on our results, we conclude that the use of AuQDs offers new opportunities for improving organic solar cell devices.

REFERENCES

1. H. Kawasaki, K. Hamaguchi, I. Osaka, R. Arakawa, *Adv. Funct. Mater*. 2011, **21**, 3508.
2. K. G. Stamplecoskie, Y. S. Chen, P. V. Kamat, *J. Phys. Chem. C* 2014, **118**, 1370.
3. J. Zheng, C. Zhang, R. M. Dickson, *Phys. Rev. Lett*., 2004, **93**, 077402.

4. T. Huang, R. W. Murray, *J. Phy. Chem. B* 2001, **105**, 12498.
5. N. Sakai, T. Tatsuma, *Adv. Mater.* 2010, **22**, 3185.
6. A. Kogo, Y. Takahashi, N. Sakai, T. Tatsuma, *Nanoscale* 2013, **5**, 7855.
7. H. Choi, Y. S. Chen, K. G. Stamplecoskie, P. V. Kamat, *J. Phys. Chem. Lett.* 2015, **6**, 217.
8. M. A. Abbas, T.-Y. Kim, S. U. Lee, Y. S. Kang, J. H. Bang, *J. Am. Chem. Soc.* 2016, **138**, 390.
9. C. W. Tang, *Appl. Phys. Lett.* 1986, **48**, 183.
10. J. Y. Kim, K. Lee, N. E. Coates, D. Moses, T. Q. Nguyen, M. Dante, A. J. Heeger, *Science* 2007, **317**, 222.
11. A. Baba, N. Aoki, K. Shinbo, K. Kato, F. Kaneko, *ACS Appl. Mater. Interfaces* 2011, **3**, 2080.
12. S. Y. Khoo, H. Yang, Z. He, J. Miao, K. C. Leong, C. M. Li, T. T. Yang Tan, *J. Mater. Chem. A* 2013, **1**, 5402.
13. C. C. D. Wang, W. C. H. Choy, C. Duan, D. D. S. Fung, W. E. I. Sha, F.X. Xie, F. Huang, Y. Cao, *J. Mater. Chem.* 2012, **22**, 1206.
14. H. A. Atwater, A. Polman, *Nature Mater.* 2010, **9**, 205.
15. E. Stratakis, E. Kymakis, *Mater. Today* 2013, **16**, 133.
16. C. Fei Guo, T. Sun, F. Cao, Q. Liu, Z. Ren, *Light: Sci. Appl.* 2014, **3**, e161.
17. X. Li, X. Ren, F. Xie, Y. Zhang, T. Xu, B. Wei, W. C. H. Choy, *Adv. Opt. Mater*. 2015, **3**, 1220.
18. G. D. Spyropoulos, M. M. Stylianakis, E. Stratakis, E. Kymakis, *Appl. Phys. Lett.* 2012, **100**, 213904.
19. C. Liu, C. Zhao, X. Zhang, W. Guo, K. Liu, S. Ruan, *J. Phys. Chem. C* 2016, **120**, 6198.
20. L. Lu, Z. Luo, T. Xu, L. Yu, *Nano Lett.* 2013, **13**, 59.
21. D. Kozanoglu, D. H. Apaydin, A. Cirpan, E. N. Esenturk, *Org. Electron.* 2013, **14**, 1720.

22. A. Pangdam, S. Nootchanat, R. Ishikaw, K. Shinbo, K. Kato, F. Kaneko, C. Thammacharoen, S. Ekgasit, A. Baba, *Phys. Chem. Chem. Phys*. 2016, **18**, 18500.

23. Z. Li, X. Zhang, C. Liu, Z. Zhang, Y. He, J. Li, L. Shen, W. Guo, S. Ruan, *J. Phys. Chem. C* 2015, **119**, 26747.

24. S. Bishnoi, V. Gupta, C. Sharma, D. Haranath, S. Naqvi, M. Kumar, G. D. Sharma, S. Chand, *Appl. Phys. Lett.* 2016, **109**, 023902.

25. J. K. Kim, M. J. Park, S. J. Kim, D. H. Wang, S. P. Cho, S. Bae, J. H. Park, B. H. Hong, *ACS Nano* 2013, **7**, 7207.

26. G. H. Kim, B. Walker, D. Zhitomirsky, J. Heo, S. J. Ko, J. Park, E. H. Sargent, J. Y. Kim, *Nano Energy* 2015, **13**, 491.

27. Y. Xia, Y. Xiong, B. Lim, S. E. Skrabalak, *Angew. Chem. Int. Ed.* 2009, **48**, 60.

28. B. J. Leever, C. A. Bailey, T. J. Marks, M. C. Hersam, M. F. Durstock, *Adv. Energy Mater*. 2012, **2**, 120.

29. G. Perrier, R. de Bettignies, S. Berson, N. Lemaître, S. Guillerez, *Sol. Energy Mater. Sol. Cells* 2012, **101**, 210.

30. G. Garcia-Belmonte, A. Munar, E. M. Barea, J. Bisquert, I. Ugarte, R. Pacios, *Org. Electron.* 2008, **9**, 847.

31. S. Woo, J. H. Jeong, H. K. Lyu, Y. S. Han, Y. Kim, *Nanoscale Res. Lett.* 2012, **7**, 1.

32. A. Ng, W. K. Yiu, Y. Foo, Q. Shen, A. Bejaoui, Y. Zhao, H. C. Gokkaya, A. B. Djurišić, J. A. Zapien, W. K. Chan, C. Surya, *ACS Appl. Mater. Interfaces* 2014, **6**, 20676.

CHAPTER IV

Enhanced Organic Thin-Film Solar Cell Efficiency via the Combination of three difference plasmonic excitations of silver nanoprisms (AgNPrs)

ABSTRACT

In this study, the combination of three different sizes and shapes, i.e. AgNPrs (R, P and B-AgNPrs) or mixed AgNPrs are used as light-trapping organic thin-film solar cells (OSCs). Mixed AgNPrs, which have three different plasmonic excitation, were included in OSCs for enhancing electric field and light scattering in broadband absorption that attributed to mutual multiple plasmonic excitations. The suitable ratio for highest broadband absorption of R, P and B-AgNPrs in mixed AgNPrs was calculated by multiple linear regression (MLR) on central composition design (CCD). Mixed AgNPrs were included in a poly(3,4ethylenedioxythiophene) :poly(styrene sulfonate) (PEDOT:PSS) thin film layer of organic thin-film solar cells (OSCs). UV–vis spectra, atomic force microscope (AFM) images, current density versus voltage properties, and the impedance spectra of the fabricated devices were measured with various concentrations of Mixed AgNPrs. The results suggest that the efficiency of the OSCs with mixed AgNPrs was higher than not only that of a reference cell without nanoparticles but also than that of OSCs with sole AgNPrs in the similar loading concentration. Finite-difference time-domain simulation explained that the electric field around the different shape AgNPrs was increased in difference mode related with incident photon-to-current efficiency of AgNPrs-loading OSCs.

INTRODUCTION

The quantum-size-effect of precious metal such as gold and silver nanoparticles (AuNPs and AgNPs) shows novel optical properties.[1] These changes are explained by the localized surface plasmon resonance (LSPR) that relates with a phenomenon of electron cloud oscillation on the surface of metallic nanoparticles.[2] These nanoparticles could generate a large of light absorption/electric field enchantment. Then, light scattering/Mie scattering is occurred due to materials size coming to nanoscale.[3] The LSPR depended on the size, shape of metallic nanoparticles that are included in environmental surrounding. Therefore, the morphology change of AuNPs/AgNPs is dramatically effective with spectroscopic properties of these materials.[4,5] The LSPR of AuNPs and AgNPs was used in many fields research such as chemical sensor,[6] medical diagonal,[7] and plasmonic solar cells.[8] Especially, these applications are interested and observed the strong optical activity to be occurring and changing in visible region.

For thin-film organic solar cells (OSCs), the poly(3-hexylthiophene-2,5-diyl) (P3HT) and phenyl-C61-butyric acid methyl ester (PCBM) are the best seller use as organic semiconductor in OSCs. This organic dye incorporated with low-band-gap has the main excitation in visible region from 400 – 650 nm.[9] However, the thin film structures of OSCs show low light absorption ability and high refection light on the flat surface of device that negatively affects with photovoltaic cells.[10] Therefore, the light harvesting method is considered for highly collecting photon within OSC, especially, in visible light. One of them, metallic nanoparticles were used for enhancing the electric flied/ light scattering enchantment by plasmonic properties as light-trapping materials. These materials could promote photocarriers in the exciton of organic dye and increase solar cells efficiency.[3,11]

In the case of AgNPs, these metallic nanoparticles were famously included in OSCs due to tuning ability of size and shape and the economy price compared with AuNPs.[12,13] Previous works in this field of plasmonic solar cells, AgNPs in different shape such as sphere,[14] prisms,[15] and plate [16] show the facility to enhance the solar cells efficiency of OSCs in visible region that confirms the successful use of AgNPs as the light-trapping material for OSCs. To open another opportunity, the broadband light absorption enhancement was considered by cooperation of different plasmonic excitation. It means that mixed different size and shape of AgNPs could promote broadband plasmonic absorption more than single type AgNPs. The plasmonic combination of mixed AgNPs could advance to promote electric field enhancement and light scattering in broadband spectrum, and enhance percent of power conversion efficiency (%PCE) more than ones size or shape of AgNPs. Previous work, mixing different shapes and types of metal nanoparticles such as spherical AgNPs and AuNPs,[17] spherical AgNPs and triangular Ag nanoprisms,[18] and Au bone-like, rod, cube, and spherical nanostructures [19] showed high effect on a large improvement efficiency of photovoltaic device more than reference cells and either AgNPs or AuNPs within OSCs.

In our work, silver nanoprisms (AgNPrs) in mixture size and shapes of circular, hexagonal and truncated triangular show different plasmonic excitations that demonstrates the strong plasmonic colour such as R-AgNPrs (red), P-AgNPrs (purple) and B-AgNPrs (blue), respectively. The mixture size and shapes of AgNPrs or "mixed AgNPrs" as different concentration ratios were considered to enhance broadband plasmonic absorption. To observe an optimum condition, all mixture ratios were designed by central composition design (CCD), and plasmonic changing were observed by UV-vis spectrophotometer. The multiple linear regression (MLR) were

used for calculation to discover a suitable condition ratio for maximum broadband absorption. After that, the optimization ratio of mixed AgNPrs was used for light-trapping materials in OSCs by blending into hole transport layer (HTL). Our results exhibit that the mixed AgNPrs in the HTL show the enhancement of the power conversion efficiency by enhancing the amount of photocarriers due to plasmonic effect within OSCs. The variation of concentrations of mixed AgNPrs within OSCs play an importance role to increase the solar cells efficiency of devices. To confirm the advantaged from cooperation of mixed AgNPrs, the incident photon to current efficiency (IPCE) and enhancement factor (E.F.) of blending a single R, P, B-AgNPrs in OSCs were compared with mixed AgNPrs in similar concentration. Moreover, finite-difference time-domain (FDTD) simulations were performed by estimating the three difference structures of AgNPrs in the OSCs to observe the variety of electric field enhancement relation with variation of AgNPrs structures.

EXPERIMENTAL

Experimental designs for mixed AgNPrs

The R-AgNPrs, P-AgNPrs and B-AgNPrs in different plasmonic excitation were purchased (Prime Nanotechnology Co., Ltd. (Thailand)). The broadband enhancement of light absorption *via* mixed AgNPrs was preliminarily observed by UV-vis spectrophotometer. The total 20 concentration ratios were designed by central composition design (CCD) that is the coded values and the actual concentration of mixed AgNPrs as shown in supporting information, Table S1. Then, peak area from 400 nm – 650 nm of previous UV-vis spectra was used as response of each experimental condition. A regression model contains with the parameters of individual, interaction and quadratic terms that were calculated using multiple linear regression

(MLR). The predicted responses (peak area in this case) were calculated using an obtained regression model and the optimized conditions was assessed by respond surface plots.

Fabrication of OSCs containing mixed AgNPrs

A schematic of the fabricated plasmonic enhancement of bulk-heterojunction OSCs *via* mixed AgNPrs is shown in Figure 1. The suitable concentration ratios of mixed AgNPrs calculated by MLR were diluted to a preferred concentration from 0.00 – 0.05 mM in deionized water. After that, mixed AgNPrs was blended with poly (3,4 ethylenedioxythiophene): poly(styrenesulfonate) (PEDOT: PSS) (Clevios, Heraeus Co.) (1 : 5 v/v) and for 1 h under ultrasonic irradiation. PEDOT:PSS loading mixed AgNPrs was deposited on indium tin oxide substrates (FINE brand, Furuuchi Co. Ltd, 10 Ω cm^2), as a HTL, by spin coating at 1000 rpm for 1 min. The thickness of the PEDOT:PSS films was approximately 100 nm (supporting information, Figure S1). The deposited PEDOT:PSS film was annealed at 120 ^oC for 20 min. Consequently, phenyl-C61-butyric acid methyl ester (PCBM) (Sigma-Aldrich) blended with poly(3-hexylthiophene) (P3HT) (Sigma-Aldrich), which were dissolved in dichlorobenzene (Sigma-Aldrich) with a P3HT :PCBM mass ratio of 1 : 0.8, was coated on the PEDOT:PSS layer as an active layer by spin coating at 1500 rpm for 1 min. The P3HT:PCBM film thickness was approximately 100 nm (supporting information, Figure S2). The deposited films were annealed at 120 ^oC for 10 min. The top aluminium electrode (thickness = ~150 nm) of OSCs was deposited on the P3HT:PCBM layer using a vacuum thermal evaporation technique. Finally, the fabricated OSCs were annealed at 150 ^oC for 45 min in a vacuum chamber.

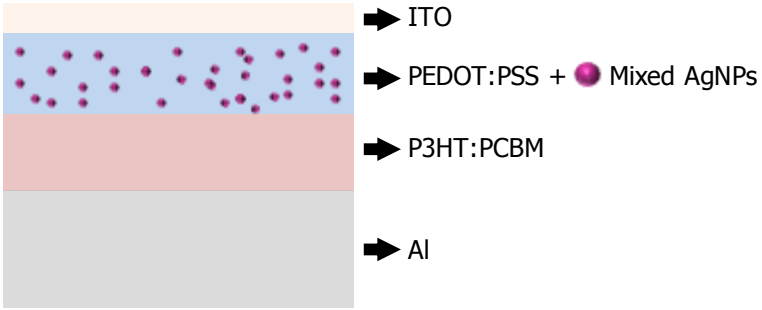

Figure 1. Schematic of the fabricated AgNPrs-enhanced OSCs.

Characterization of PEDOT:PSS films loading AgNPrs and OSCs with AgNPrs

The UV–vis absorption of mixed AgNPrs solution, PEDOT:PSS and AgNPr-loaded PEDOT:PSS films was investigated using a UV–vis spectrometer (V-650, Jasco). The morphology of AgNPrs dispersions on the surface of PEDOT:PSS films was observed by AFM microscopy (SPM-9600, Shimadzu). Photovoltaic parameters of OSCs with/without AgNPrs were investigated under solar simulator light irradiation (HAL-C100, 100 W compact xenon light source, Asahi Spectra) using a precision source-meter unit (B2901A, Agilent). Moreover, the effect of mixed AgNPrs in OSCs was explained by impedance spectrometer (PARSTAT 4000, Princeton Applied Research) under solar light illumination.

RESULTS AND DISCUSSION

The plasmonic effect on size and shape variation of AgNPrs

The different plasmonic activity depends on size and shape of AgNPrs in system.[4] Briefly, the optical expressions of AgNPrs in the red (R-AgNPrs), purple (P-AgNPrs) and blue (B-AgNPrs) were used to easily classify. To investigate the relation of morphology and plasmonic extrication, the UV-vis spectra of colloidal R-AgNPrs, P-AgNPrs and B-AgNPrs, as shown in Figure 2d, demonstrate an absorbance maximum (λ_{max}) or dipole plasmon resonance at 513, 573 and 667 nm, respectively. The dipole

plasmon resonance plays an important role to controls the main activity of optical properties also electric filed enhancement of AgNPrs. TEM image of R-AgNPrs (Figure 2a) demonstrates the shape and size of single circular AgNPrs around 20 - 50 nm that show the lowest λ_{max} than P-AgNPrs and B-AgNPrs, respectively. The shifts of λ_{max} from short wavelength to long wavelength of light absorption are due to increase of AgNPrs size that declines a frequency of dipole plasmon resonance.[4,20,21] According to morphology of AgNPrs, the majority size of circular, hexagonal and truncated triangular shapes in large particles is increased from 50 nm to 80 nm, approximately, that could observe in TEM image of Figure 2b and 2c from P-AgNPrs and B-AgNPrs, respectively.

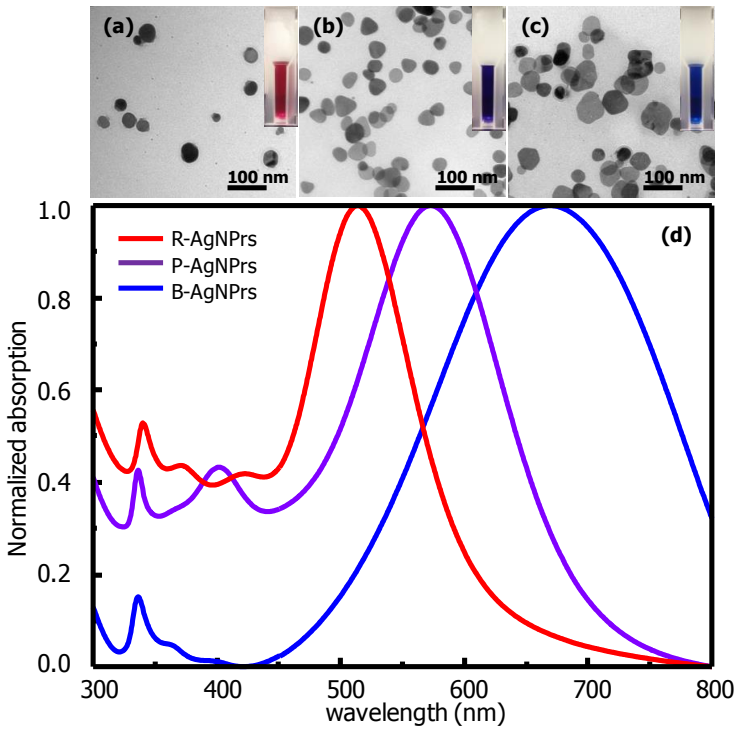

Figure 2. TEM image of (a) R-AgNPrs, (b) P-AgNPrs, (c) B-AgNPrs and (d) the UV-vis spectra of three different plasmonic excitation of AgNPrs dispersion in water. The scale bars indicate 100 nm.

Optimized condition of mixed AgNPrs by CCD experiments for enhancing light absorption

The colloidal solutions of AgNPrs with the three different plasmonic excitations as shown in Figure 2 was used here to enhancing light absorption of our fabricated OSCs However, the AgNPrs show the narrow absorption bands which do not overlap the band excitation of the organic semiconductor (P3HT:PCBM). Therefore, the mixing protocol of the AgNPrs in the P3HT:PCBM layer might promote a broadband light absorption enhancement, which is mutually of multiple plasmonic excitations. To assess the maximum enhancement phenomenon, the appropriate concentration ratios of R-AgNPrs, P-AgNPrs and B-AgNPrs is required. In this work, the central composite design (CCD) approach was performed. This approach was used to determine the mixing conditions which give the highest peak area of UV-vis spectrum. This obtained peak area can be used as an index to estimate the enhancement of light absorption. In the case, only peak area of UV-vis spectrum from 400 nm – 650 nm of mixed AgNPrs was considered (Supporting information, Figure S3 and Table S2). The regression function is shown below.

$$Y_{\text{peak area}} = 119.27 + 27.04X_1 + 25.22X_2 + 17.17X_3 - 2.18X_1^2 + 1.06X_2^2 + 0.59X_3^2 - 0.21X_{12} - 0.11X_{13} - 0.16X_{23} \quad .....(1)$$

Where, X_1, X_2 and X_3 are linear terms corresponding to concentration of R-AgNPrs, P-AgNPrs and B-AgNPrs, respectively. X_1^2, X_2^2, X_3^2 and X_{12}, X_{13}, X_{23} are quadratic terms and interaction terms of the parameters. From the regression model, it can be noticed that the regression coefficients of the linear terms (X_1, X_2, and X_3) is largely positive. This suggests that the respond (peak area) directly depend on the concentration of R, P and B-AgNPrs in a linear relationship. The interaction terms

including X_{12}, X_{13} and X_{23} show very low coefficient in the regression model. This might be concluded that there are no synergic effects between R, P and B-AgNPrs to the obtained peak area. Therefore, the increase of peak area comes from increasing concentration of each R, P and B-AgNPrs. The regression coefficients of quadratic terms also show insignificantly compared to the linear terms. This suggests that the optimum condition is the same point with the maximum concentration of R, P and B-AgNPrs, which can load to system. To assess optimum condition, the response surface plot of the peak area was shown in Figure S4, supporting information. It shows that the higher concentrations of AgNPrs lead to the larger responses (peak area). This surface plot is in good agreement with the calculated coefficient of the regression model. The highest response (peak area) was estimated by responsive surfaces of central composition (Supporting information, Figure S5) that show concentrations at 0.10, 0.10 and 0.10 mM of R-AgNPrs, P-AgNPrs and B-AgNPr, respectively. This ratio was confirmed by mixed AgNPrs in previous concentration ratio that show the high accuracy data of peak area between calculation and experiment (supporting information, Table S3). The UV-vis spectrum and digital photograph of mixed-AgNPrs in previous ratio show in Figure 3.

Effect of AgNPrs in UV–vis light absorption

Mixed AgNPrs can easily be dispersed in water soluble PEDOT:PSS due to soluble starch as a stabilizing agent on surface of AgNPrs.[4] The effect of mixed AgNPrs when materials are dispersed in PEDOT:PSS films were investigated. The UV–vis light absorption of PEDOT:PSS films after blending with mixed AgNPrs was measured with different concentrations of mixed AgNPrs, as shown in Figure 4. The

UV–vis spectra show that increasing light absorption of PEDOT:PSS films from 400 – 650 nm is clearly altered by varying the concentration of mixed AgNPrs.

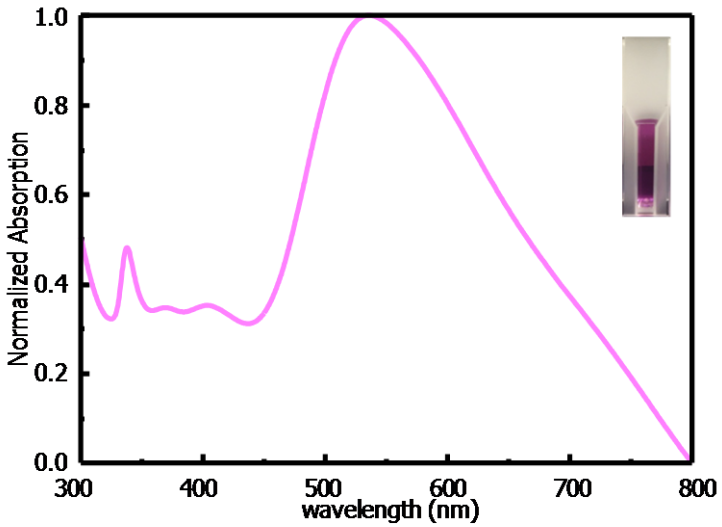

Figure 3. the UV-vis spectrum of mixed AgNPs (insert digital photograph) at concentration ratio of 1:1:1 show the broadband light absortion calculating by the regression model on central composition design.

To consider of broadband spectrum from 400 – 800 nm, the rising of absorption spectra is directly relative with the amount of AgNPrs in PEDOT:PSS film. The increasing of light absorption depends on the effect of LSPR and Mie scattering of AgNPrs.[3] The result shows that increasing mixed AgNPrs until 0.03 mM could promote a large enhancement more than other concentrations. However, when the concentrations of mixed AgNPrs were increased to 0.04 and 0.05 mM, the light absorption began to decrease, indicating that certain aspects of some mixed AgNPrs disappear from the film. To study this phenomenon, AFM images of the films were observed as shown in Figure 5. The unique AgNPrs shape such as circular, hexagonal and truncated triangular cannot be observed. The AgNPrs have a high possibility blending inside PEDOT:PSS film or transferring from original shape to aggregated particles due to mixing process and changing environment. According to previous

supposition, a small amount of aggregated AgNPrs on smooth surface of PEDOT:PSS film can be observed at 0.01, 0.02 and 0.03 mM.

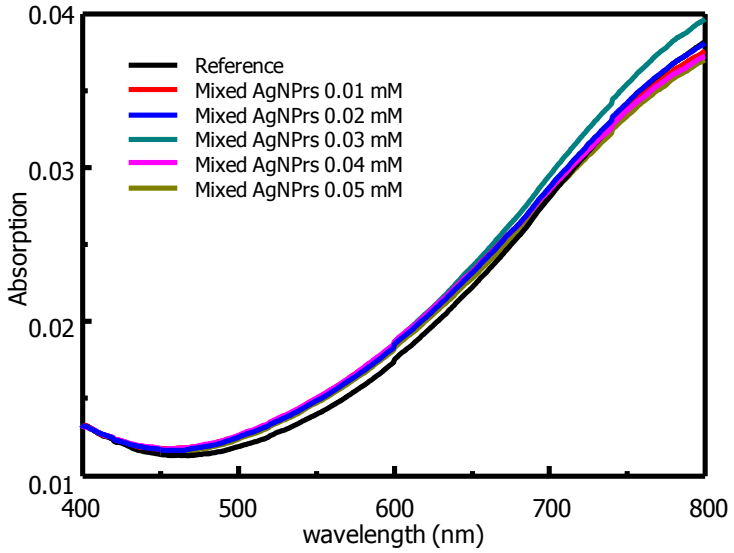

Figure 4. the UV-vis spectra showing the effect of mixed AgNPrs concentration on the absorption of PEDOT:PSS films.

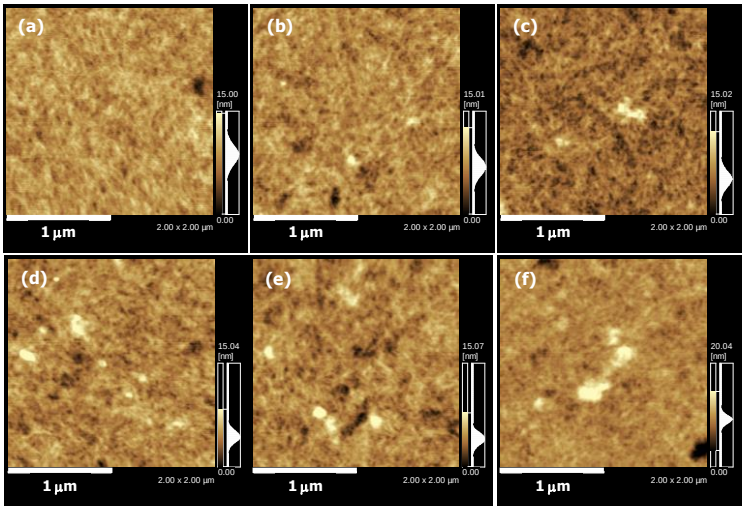

Figure 5. AFM images of PEDOT:PSS films after the addition of mixed AgNPrs via a blending process. (a) 0 mM mixed AgNPrs, (b) 0.01 mM mixed AgNPrs, (c) 0.02 mM mixed AgNPrs, (d) 0.03 mM mixed AgNPrs, (e) 0.04 mM mixed AgNPrs and (f) 0.05 mM mixed AgNPrs.

However, when the concentrations were increased to 0.04 and 0.05 mM, a large AgNPrs aggregate and clusters were observed on the PEDOT:PSS films. Normally, aggregation of nanoparticles is easy to occur by interfering environment of nanoparticles such as temperature, concentration ionic strength and solubility. These parameters could promote nanoparticles to easily concomitance to aggregated particles for reducing the surface energy within the system and precipitation in finally.[22] Therefore, the aggregation of mixed AgNPrs in the system at a high concentration is reasonable. Moreover, the plasmonic properties of AgNPrs will be decreased when the size of particles coming to microscale. Therefore, decreasing in UV-vis spectra at high concentration of mixed AgNPrs were affected from a large aggregated particles that disappear particles from PEDOT:PSS film and reduce absorption enhancement.

Effect of mixed AgNPrs in OSCs

Figure 6 and Table 1 respectively show current density versus voltage (*J*–*V*) properties and photovoltaic parameters of the fabricated OSCs with/without of mixed AgNPrs in PEDOT:PSS films. The standard deviation was obtained by measuring three different devices of the same structure. To study the effect of mixed AgNPrs, the concentration of mixed AgNPrs in PEDOT:PSS was increased from 0.01 mM to 0.05 mM. The reference cells without mixed AgNPrs (mixed AgNPrs at 0 mM) exhibit a short-circuit current density (J_{SC}) of 7.5±0.3 mA/cm^2, an open-circuit voltage (V_{OC}) of 0.60±0.01 V, a fill factor (FF) of 0.58±0.02, and a solar cell efficiency (η) of 3.46±0.08 %. Hence, the increasing η (%) of approximately 6% were obtained in the case of 0.03 mM of mixed AgNPrs. However, the OSCs with mixed AgNPrs at 0.04 mM and 0.05 mM exhibited a decrease in J_{SC} and η in comparison to the reference cell. This can be explained by the following two reasons. Firstly, the large aggregation of mixed

AgNPrs in PEDOT:PSS films (AFM image, Figuges. 5e and 5f) caused a connection between the anode and active layer, resulting in the short circuit in the system. Secondly, the light-trapping efficiency due to plasmonic properties of metal nanoparticles were quenched when the particles size are growth to bulk material.

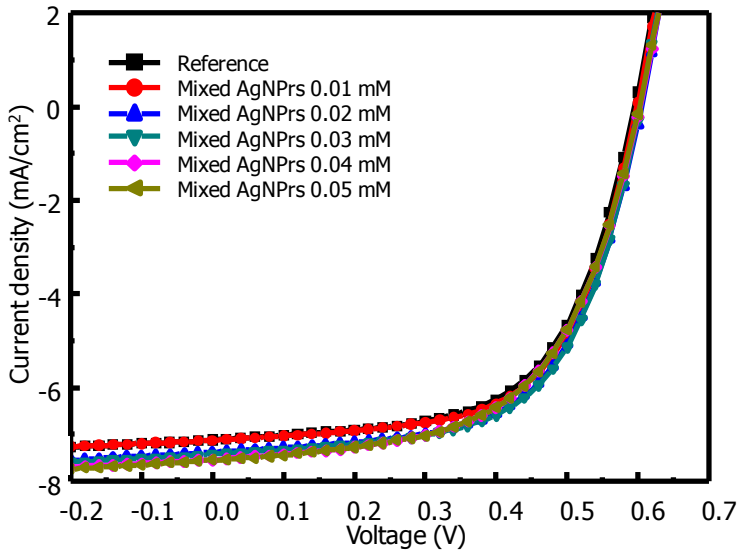

Figure 6. *J–V* properties of OSCs with mixed AgNPs in OSCs blended with PEDOT:PSS compared with reference cells.

Table 1 The photovoltaic parameters of OSCs under different conditions.

	J_{SC} (mA cm^{-2})	V_{OC} (V)	FF	η(%)
Reference cells	7.5±0.3	0.60±0.01	0.58±0.02	3.46±0.08
Mixed AgNPs 0.01 mM	7.2±0.1	0.601±0.002	0.61±0.02	3.54±0.07
Mixed AgNPs 0.02 mM	7.5±0.1	0.604±0.001	0.61±0.01	3.67±0.09
Mixed AgNPs 0.03 mM	7.48±0.09	0.602±0.003	0.611±0.004	3.67±0.03
Mixed AgNPs 0.04 mM	7.5±0.2	0.60±0.01	0.58±0.02	3.49±0.01
Mixed AgNPs 0.05 mM	7.53±0.02	0.600±0.002	0.58±0.01	3.48±0.07

In contrast, V_{OC} was not significantly altered. The results indicate that the mixed AgNPrs increased photocarriers by increasing light intensity within OSCs, and did not affect the energy diagram of P3HT:PCBM layers. To more investigate the interfacial properties of the OSCs were measured by impedance spectroscopy that is a useful technique for electron transport and recombination of photovoltaic cells.[23,24] The Nyquist plots of the impedance spectra of the mixed AgNPrs-loaded OSCs, and OSCs without the mixed AgNPrs, under solar light illumination as shown in Figure 8. A simple circuit model as shown in the inset as single was used to explain that semi-circle curves were observed at 0.03 mM of mixed AgNPrs. In this model, the R_s circuit element represents resistive losses in the ITO and PEDOT:PSS or PEDOT:PSS-mixed AgNPrs that corresponds to the intersection of the semicircles.[25] The R_s value of the mixed AgNPrs loaded OSCs is slightly smaller than those of the OSCs without mixed AgNPrs. It indicates that the resistance of the PEDOT:PSS layer was decreased by loading with mixed AgNPrs. In our previously report, the small among of metal nanoparticles in OSCs shows significant to reduce R_s value.[8] The Constant phase element (CPE) in circuit model is used to explain a distribution of relaxation time at interfaces and nearly same as the differential capacitance.[25] The R_{ct} value represents the bulk resistance of P3HT:PCBM,[25-27] which decreased in the following order: OSCs without mixed AgNPrs (7.7 Ω) and OSCs with mixed AgNPrs (7.3 Ω). The decline of R_{ct} is directly affected from the increase in the number of charge carriers in the P3HT:PCBM layers. This result suggests that the mixed AgNPrs generated more photocarriers in the P3HT:PCBM layer.

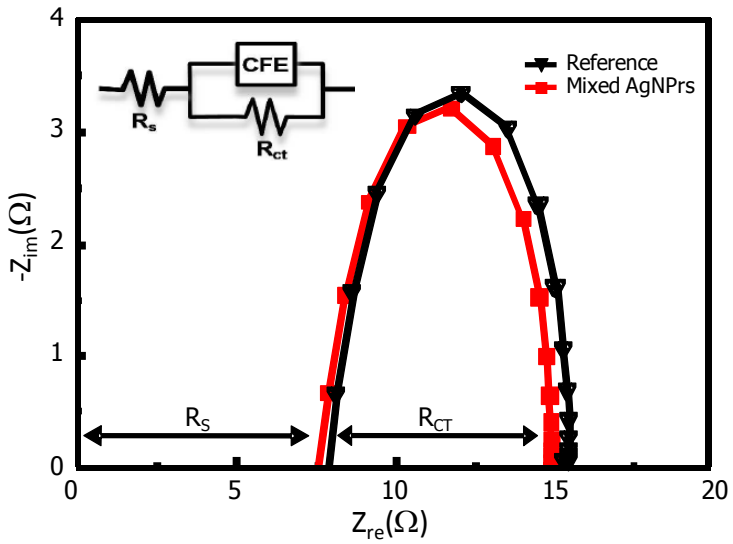

Figure 7. The Nyquist plots of the OSCs without mixed AgNPrs and the mixed AgNPrs -loaded OSCs at 0.03 mM under solar light illumination.

The mechanism of Mixed AgNPs for improvement the efficiency of OSCs

To observe in the detail of enhancement mechanism, light-trapping effect of mixed AgNPs on OSCs for increasing solar cell efficiency were investigated by the incident photon to current efficiency (IPCE) of fabricated OSCs as shown in Figure 8a. The mixed AgNPrs exhibit higher IPCE also %PCE comparing with individual AgNPrs (R-AgNPrs, P-AgNPrs and B-AgNPrs) in the similar concentration 0.03 mM and reference OSCs (supporting information, Figure S6). To gain the understanding, the effect of plasmonic enhancement of AgNPrs on OSC was considered by the enhancement factor (E.F.), which is the ratio of IPCE of AgNPrs-loading to that of the reference OSC without AgNPrs as shown in Figure 8b. The E.F. shows the strong enhancement intensity of B more than R and P-AgNPrs-loading in OSCs, respectively from 650 – 800 nm. However, these enhancement patterns show the red shift that is difference from original plasmon band of colloidal AgNPrs in deionized water as shown in Figure 2d. The results suggest that AgNPrs aggregations are occurred in fabrication devices. The small particle size of nanoparticles can promote the high degree of particles aggregation

more than the large nanoparticles for reducing surface energy.[22] Therefore, the R-AgNPrs show a large of particles aggregation and give a large enhancement as well as B-AgNPrs. On the other hand, the large size of AgNPrs have the low degree of aggregation, which they are still conservative the some original particles. Therefore, some enchantment peaks of B and P-AgNPrs were observed from 450-650 nm. Surprisingly, mixed-AgNPrs-loading in OSCs demonstrate the broadband enchantment due to variety of size and shape from mixing AgNPrs that acts in boradband light-havesting from 450 – 800 nm. This result confirms a large range of the light absorption that is increase the photocarriers and %PCE. Moreover, the small enhancement peak at 350 and 430 nm are unclear explanation that might come from the out-of-plane quadrupole plasmon resonance of AgNPrs [4,28] and dipole plasmon resonance of spherical AgNPs [20,29] due to shape transforming from AgNPrs to AgNPs by etching process of polystyrene sulfonate (PSS) as strong acidic,[30] respectively.

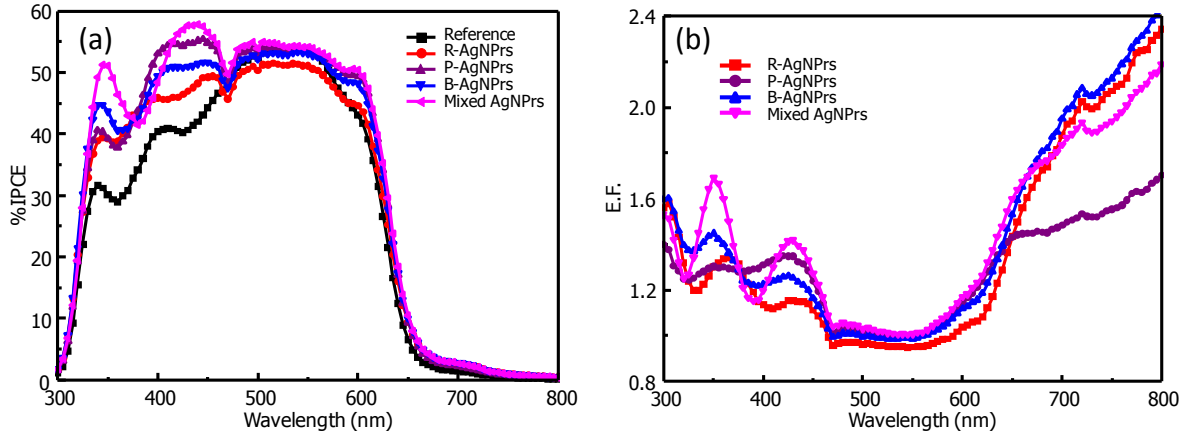

Figure 8. (a) Incident photon-to-current efficiency (IPCE) and (b) enhancement factor (E.F.) showing the effect of particle shape between mixed AgNPs and sole AgNPs on OSCs in similar concentration.

CONCLUSIONS

We successfully used mixed AgNPrs consisting with R, P and B-AgNPrs as light-trapping materials for broadband light-harvesting in OSCs. By experimental design, the multiple linear regression (MLR) on central composition design (CCD) were used to estimate the hightest peak area from difference concentration ratios of mixed AgNPrs. The result suggest that the sutible concentration ratio of mixed AgNPrs could make a large of broadband absorption in the same range of photon exciton in organic dye of OSCs by mutually of multiple plasmonic excitations. After that, mixed AgNPrs at 0.03 mM were included in hole transport layer of OSCs that could promote the increasing 6% of PCE when compared with reference. However, the high loading concentration of mixed AgNPrs could make the problem with the efficiency of OSCs due to particles aggregation inside fabrication devices. Moreover, the cooperation of R, P and B-AgNPrs in mixed AgNPrs shows the higher efficiency than that of OSCs with sole AgNPrs in the similar loading concentration. The improveing of PCE affects from raise in the number of charge carriers in the P3HT:PCBM layers by plasmonic effect of mixed AgNPrs. We demonstrate the mechanism of mixed AgNPrs for enhancement OSCs by incident photon-to-current efficiency (IPCE). The results suggest that the preferment of mixed AgNPrs for broadband light-havesting is more than R, P and B-AgNPrs due to the more variation mixture in different size and shape of AgNPrs. Surprisingly, the plasmonic excitations at 350 nm and 430 nm from the dipole plasmon of spherical AgNPs and quadrupole plasmon resonance of AgNPrs (*i.e.* circular, hexagonal and truncated triangular), respectively, were explained by FDTD simulations. Based on our results, we conclude that the use of mixed AgNPrs offers new opportunities for improving organic solar cell devices.

REFERENCES

1. K. L. Kelly, E. Coronado, L. L. Zhao and G. C. Schatz, *J Phy. Chem. B*, 2003, **107**, 668-677.
2. K. M. Mayer and J. H. Hafner, *Chem. Rev.*, 2011, **111**, 3828-3857.
3. H. A. Atwater and A. Polman, *Nat Mater*, 2010, **9**, 205-213.
4. T. Parnklang, C. Lertvachirapaiboon, P. Pienpinijtham, K. Wongravee, C. Thammacharoen and S. Ekgasit, *RSC Adv*., 2013, **3**, 12886-12894.
5. P. Pienpinijtham, C. Thammacharoen and S. Ekgasit, *Macromol. Res.*, 2012, **20**, 1281-1288.
6. S. Vantasin, P. Pienpinijtham, K. Wongravee, C. Thammacharoen and S. Ekgasit, *Sens. Actuator B-Chem.*, 2013, **177**, 131-137.
7. Y. Hsiangkuo, G. K. Christopher, H. Hanjun, M. W. Christy, A. G. Gerald and V.-D. Tuan, *Nanotechnology*, 2012, 23, 075102.
8. A. Pangdam, S. Nootchanat, R. Ishikawa, K. Shinbo, K. Kato, F. Kaneko, C. Thammacharoen, S. Ekgasit and A. Baba, *Phys. Chem. Chem. Phys.*, 2016, **18**, 18500 - 18506.
9. M. T. Dang, L. Hirsch and G. Wantz, *Adv. Mater.*, 2011, **23**, 3597-3602.
10. J. Cai and L. Qi, *Mater. Horiz.*, 2015, **2**, 37-53.
11. J. You, X. Li, F. Xie, W. E. I. Sha, J. H. W. Kwong, G. Li, W. C. H. Choy and Y. Yang, *Adv. Energy Mater.*, 2012, **2**, 1203-1207.
12. P. C. Naha, K. C. Lau, J. C. Hsu, M. Hajfathalian, S. Mian, P. Chhour, L. Uppuluri, E. S. McDonald, A. D. A. Maidment and D. P. Cormode, *Nanoscale*, 2016, **8**, 13740-13754.
13. K.-S. Lee and M. A. El-Sayed, *J. Phys. Chem. B*, 2006, **110**, 19220-19225.
14. H. Choi, J.-P. Lee, S.-J. Ko, J.-W. Jung, H. Park, S. Yoo, O. Park, J.-R. Jeong, S. Park and J. Y. Kim, *Nano Lett.*, 2013, **13**, 2204-2208.

15.A. P. Kulkarni, K. M. Noone, K. Munechika, S. R. Guyer and D. S. Ginger, *Nano Lett.*, 2010, **10**, 1501-1505.

16.H.-L. Hsu, T.-Y. Juang, C.-P. Chen, C.-M. Hsieh, C.-C. Yang, C.-L. Huang and R.-J. Jeng, *Sol. Energy Mater. Sol. Cells*, 2015, **140**, 224-231.

17.L. Lu, Z. Luo, T. Xu and L. Yu, *Nano Lett.*, 2012, **13**, 59-64.

18.X. Li, W. C. H. Choy, H. Lu, W. E. I. Sha and A. H. P. Ho, *Adv. Funct. Mater.*, 2013, **23**, 2728-2735.

19.J. Hao, Y. Xu, S. Chen, Y. Zhang, J. Mai, T.-K. Lau, R. Zhang, Y. Mei, L. Wang, X. Lu and W. Huang, *Opt. Commun*., 2016, **362**, 50-58.

20.K. Wongravee, T. Parnklang, P. Pienpinijtham, C. Lertvachirapaiboon, Y. Ozaki, C. Thammacharoen and S. Ekgasit, *Phys. Chem. Chem. Phys*, 2013, **15**, 4183-4189.

21.K. Nitinaivinij, T. Parnklang, C. Thammacharoen, S. Ekgasit and K. Wongravee, *Anal. Methods*, 2014, **6**, 9816-9824.

22.Y. Xia, Y. Xiong, B. Lim and S. E. Skrabalak, *Angew. Chem. Int. Ed.*, 2009, **48**, 60-103.

23.S. Nho, G. Baek, S. Park, B. R. Lee, M. J. Cha, D. C. Lim, J. H. Seo, S.-H. Oh, M. H. Song and S. Cho, *Energ. Environ. Sci.*, 2016, **9**, 240-246.

24.T.-W. Zeng, I. S. Liu, F.-C. Hsu, K.-T. Huang, H.-C. Liao and W.-F. Su, *Opt. Express*, 2010, **18**, A357-A365.

25.B. J. Leever, C. A. Bailey, T. J. Marks, M. C. Hersam and M. F. Durstock, *Adv. Energy Mater.*, 2012, **2**, 120-128.

26.G. Perrier, R. de Bettignies, S. Berson, N. Lemaître and S. Guillerez, *Sol. Energy Mater. Sol. Cells*, 2012, **101**, 210-216.

27.G. Garcia-Belmonte, A. Munar, E. M. Barea, J. Bisquert, I. Ugarte and R. Pacios, *Org. Electron.*, 2008, **9**, 847-851.

28.T. Parnklang, B. Lamlua, H. Gatemala, C. Thammacharoen, S. Kuimalee, B. Lohwongwatana and S. Ekgasit, *Mater. Chem. Phys.*, 2015, **153**, 127-134.

29.S. W. Baek, J. Noh, C.-H. Lee, B. Kim, M.-K. Seo and J.-Y. Lee, *Sci. Rep.*, 2013, **3**, 1726.

30.J. W. Jung, J. U. Lee and W. H. Jo, *J. Phy. Chem. C.*, 2010, **114**, 633-637.

CHAPTER V

CONCLUSIONS

To obtain broadband light-harvesting, plasmonic properties of gold and silver nanoparticles (AuNPs and AgNPs) were used as light-trapping materials in OSCs. Based on solubility and dispersion of metal nanoparticles in the media, these materials were suitable to include in the hole transport layer of OSCs. By engineering nanostructures, the plasmonic properties (*i.e.* LSPR and Mie scattering) were tuned for matching with the photon excitation of active layer of OSCs. The light absorption and scattering were enhanced by these phenomena that could promote photocarriers and increased the solar cell efficiency. The combination of size and shape of metal nanoparticles opens the opportunities for broadband light absorption and novel photovoltaic systems.

In our work, the combination of nanothorn and core shell structure of urchin-like gold nanoparticles (UL-AuNPs) and combination of different plasmonic excitations of silver nanoprisms (Mixed-AgNPrs) showed the broadband light-harvesting in visible region. Moreover, we demonstrated significance of broadband light-harvesting with UL-AuNPs and mixed-AgNPrs at suitable concentrations that could improve solar cell efficiency of OSCs more than metal nanoparticles with narrow band light absorption (*i.e.* spherical AuNPs and AgNPrs). The enhancement of the efficiency with UL-AuNPs and mixed-AgNPrs was up to 5.86 and 6.06 %, respectively comparing with reference cells.

Furthermore, we open the opportunity of broadband light-harvesting in OSCs using gold quantum dot (AuQDs) for light-converting materials form near ultraviolet to visible region by photoluminescence. The quantum size effect of gold quantum dot played an importance role for promoting photoluminescence when the gold cluster size is less than 2 nm. The three types of AuQDs (B,G and R-AuQDs) in different light emission (blue, green

and red) were included in OSCs. The results suggested that G-AuQDs at suitable concentration gave the highest solar cell efficiency up to 10% due to matching of light emission from G-AuQDs and absorption of the active layer.

SUGGESTIONS FOR FUTURE WORK

1. The aggregation of nanoparticle systems makes many problems in OSCs (*i.e.* generating short circuit current, increasing R_S, decreasing R_{Sh} and reducing both plasmonic and fluorescence properties from metal nanoparticles). By directly mixing metal nanoparticles in hole transport layer, this procedure initiates a concomitance of nanoparticles also in the mixing solution. Therefore, metal nanoparticles should avoid directly mixing process in solution.
2. To obtain the advantage of broadband light-harvesting, the combination of plasmonic properties in visible regions of gold or silver nanoparticles and fluorescence properties of gold quantum dots should be investigated and optimized (*i.e*. loading concentration and position in OSCs).

APPENDICES

APPENDIX A

SUPPORTING INFORMATION FOR CHAPTER II

Effect of urchin-like gold nanoparticles in organic thin-film solar cells

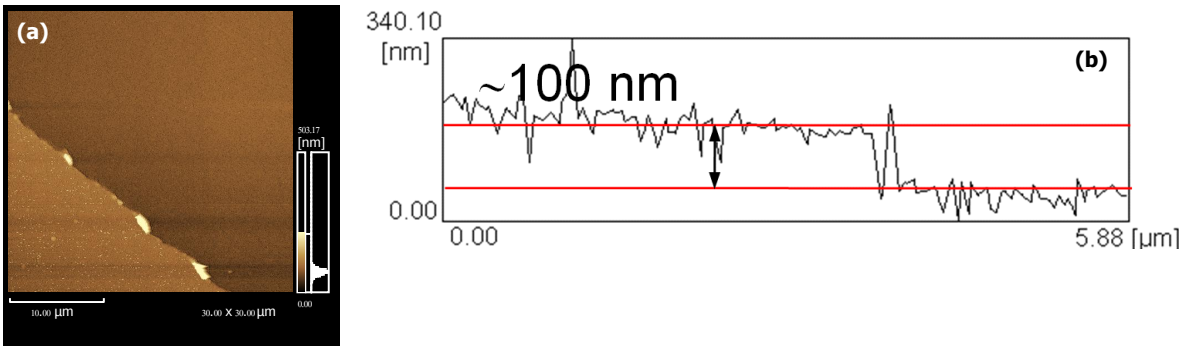

Figure S1. (a) AFM images of scratched PEDOT:PSS film on ITO glass and (b) height profile of PEDOT:PSS film-ITO glass surface. The average thickness is ca. 100 nm.

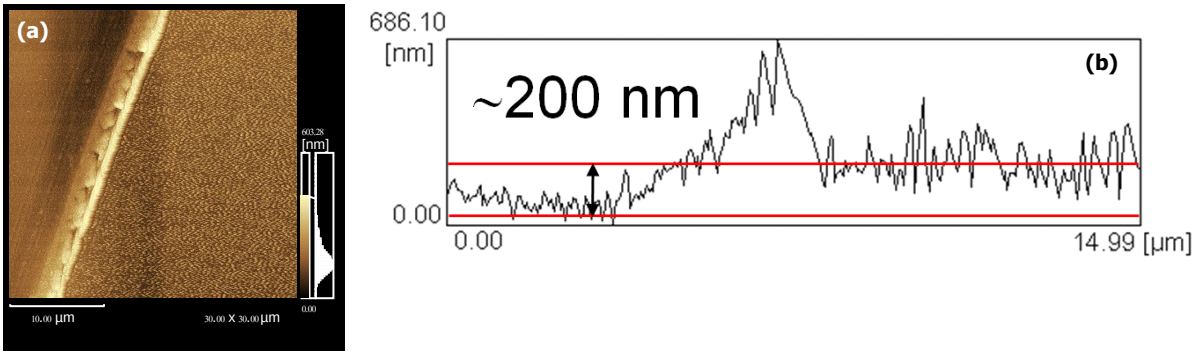

Figure S2. (a) AFM images of scratched P3HT:PCBM/PEDOT:PSS on ITO glass and (b) height profile of P3HT:PCBM/PEDOT:PSS-ITO glass surface The average thickness of P3HT:PCBM/PEDOT:PSS films is ca. 200 nm.

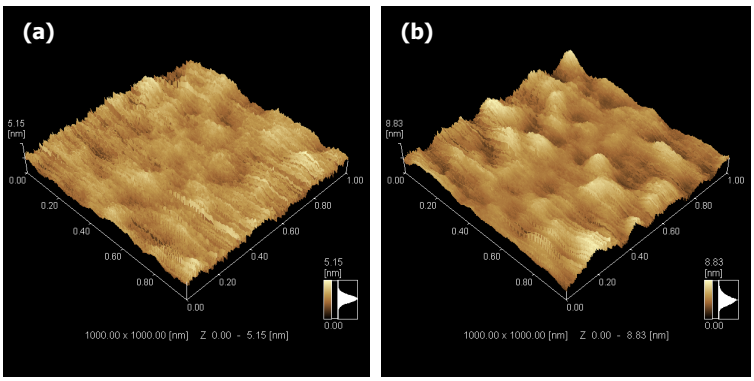

Figure S3. AFM images of the P3HT:PCBM/PEDOT:PSS/ITO glass film surface (a) without UL-AuNPs and (b) with UL-AuNPs at 0.1 mM in the P3HT:PCBM layer.

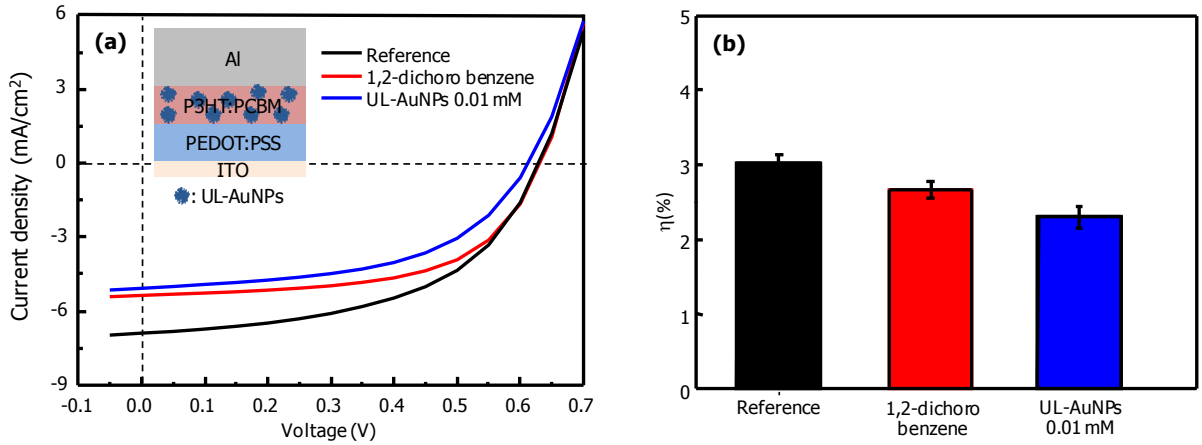

Figure S4 (a) J-V properties of (i) reference cell without UL-AuNPs, (ii) reference cell blended with 1,2-dichloro benzene (without UL-AuNPs) in P3HT:PCBM layer, and (i) OSC blended with 0.01 mM UL-AuNPs (in 1,2-dichloro benzene) in P3HT:PCBM layer and (b) the solar cell efficiency (η (%)) of each OSC.

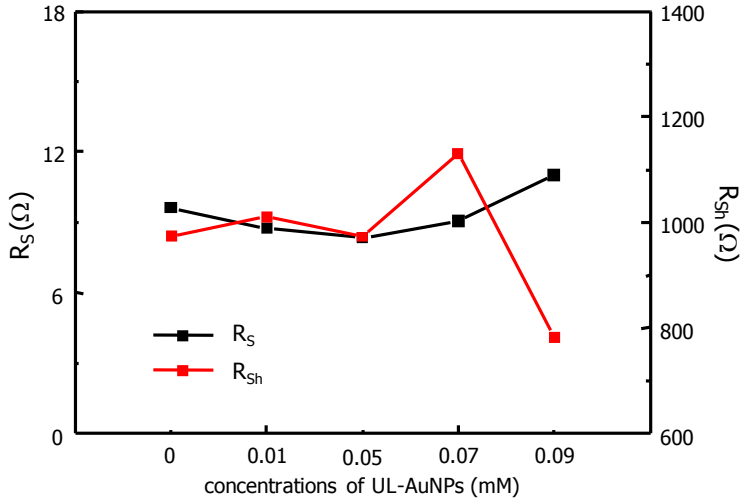

Figure S5 The series resistance (R_s) and shunt resistance (R_{sh}) of OSCs blended with ULAuNPs in PEDOT:PSS layer as a function of the concentration.

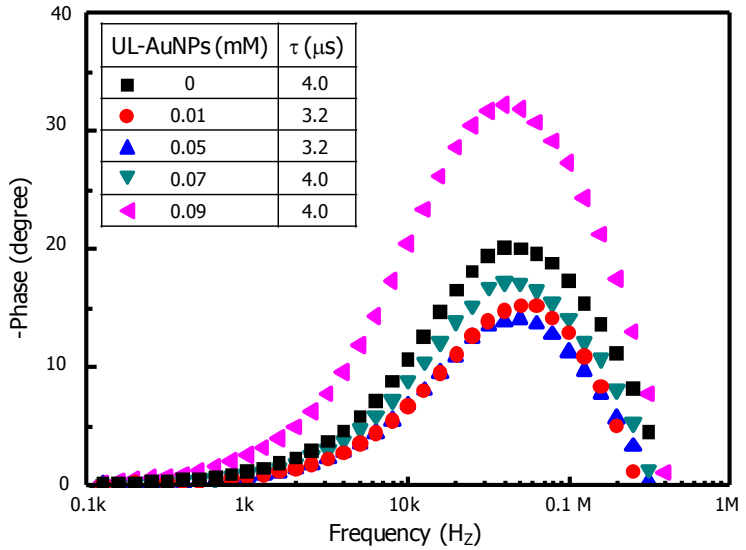

Figure S6. Bode plots of OSCs at varied concentration of UL-AuNPs in PEDOT:PSS film. The insert table shows the electron lifetime (τ)

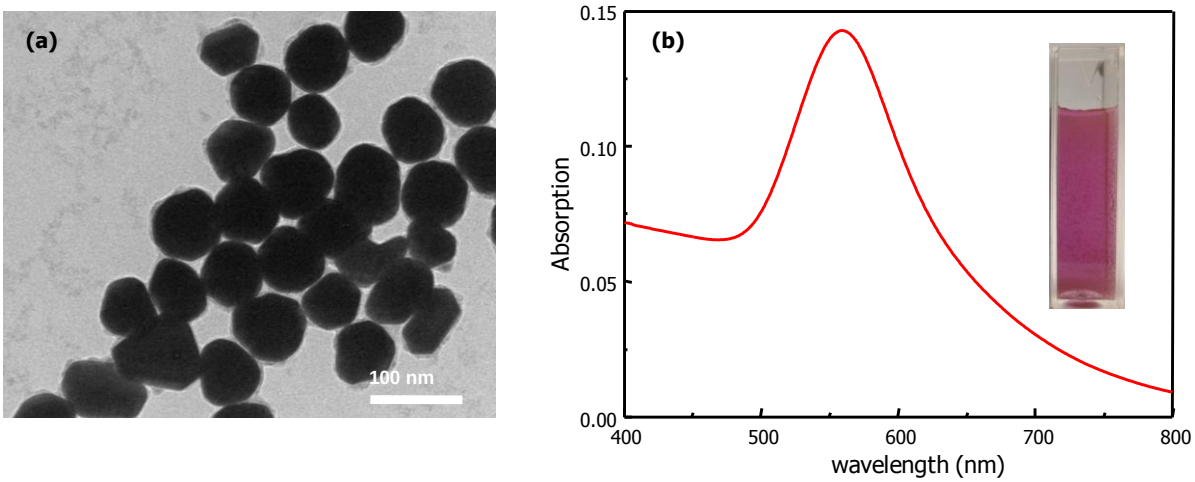

Figure S7. (a) TEM images of spherical AuNPs and (b) the UV-vis spectrum of UL-AuNPs at 0.05 mM. The scale bar indicates 100nm.

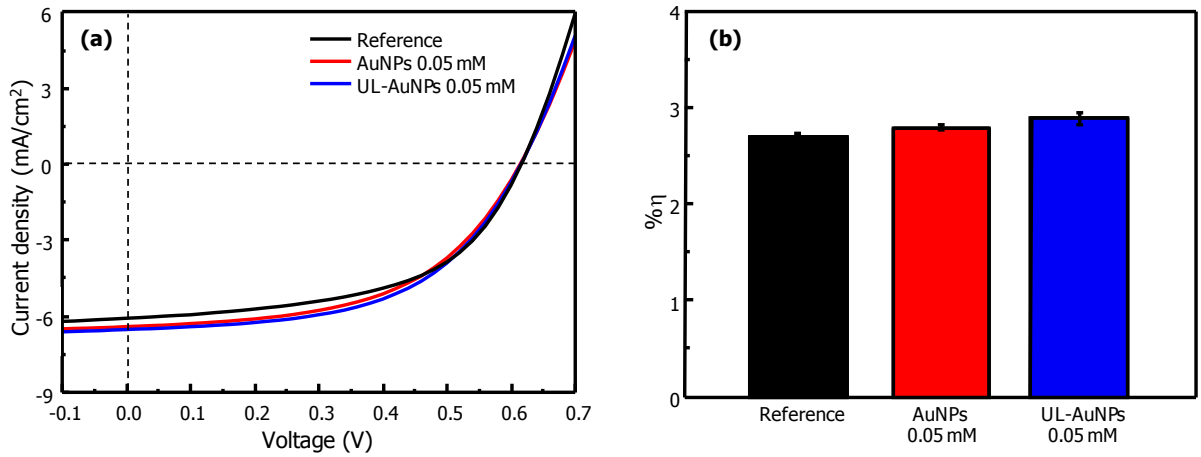

Figure S8. (a) J-V characteristic of reference OSC (without gold nanoparticles), OSC with spherical UL-AuNPs in PEDOT:PSS film, and OSC with UL-AuNPs in PEDOT:PSS film, and (b) the solar cell efficiency (η(%))

APPENDIX B

SUPPORTING INFORMATION FOR CHAPTER III

Investigation of Gold Quantum Dots Enhanced Organic Thin Film Solar Cells

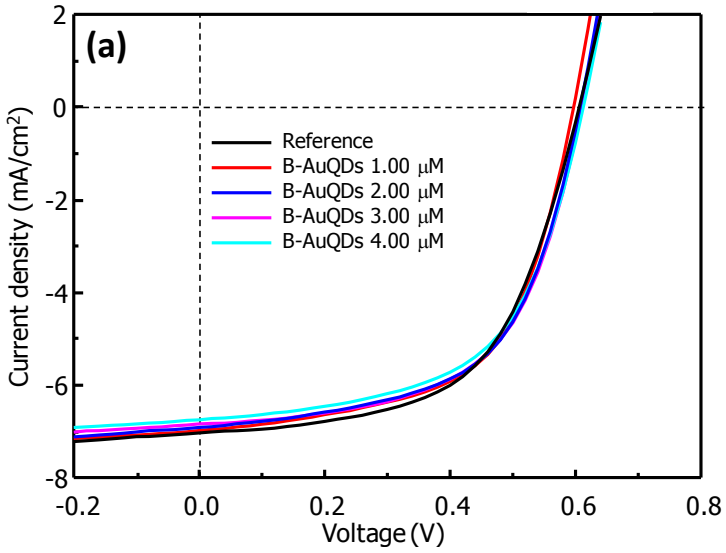
(a)
Reference
B-AuQDs 1.00 μM
B-AuQDs 2.00 μM
B-AuQDs 3.00 μM
B-AuQDs 4.00 μM
Current density (mA/cm²)
Voltage (V)
2
0
-2
-4
-6
-8
-0.2
0.0
0.2
0.4
0.6
0.8

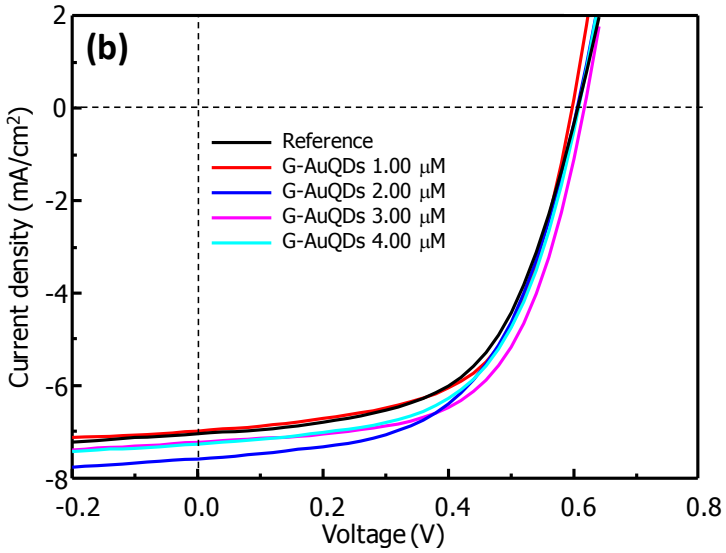
(b)
Reference
G-AuQDs 1.00 μM
G-AuQDs 2.00 μM
G-AuQDs 3.00 μM
G-AuQDs 4.00 μM
Current density (mA/cm²)
Voltage (V)
2
0
-2
-4
-6
-8
-0.2
0.0
0.2
0.4
0.6
0.8

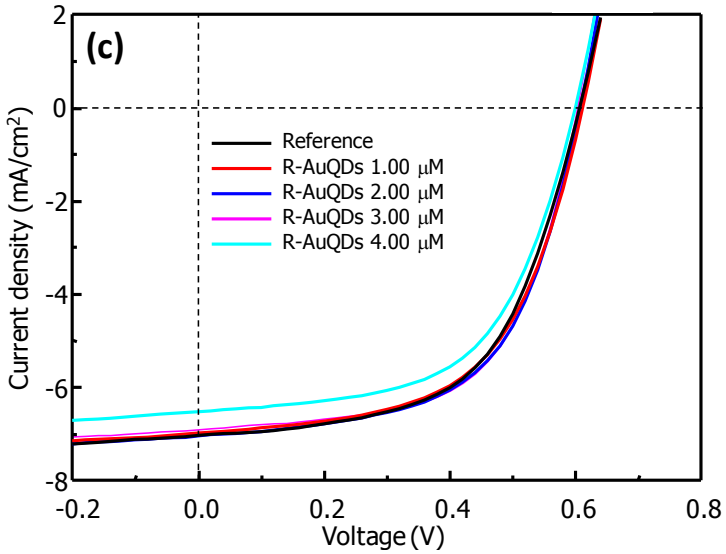
(c)
Reference
R-AuQDs 1.00 μM
R-AuQDs 2.00 μM
R-AuQDs 3.00 μM
R-AuQDs 4.00 μM
Current density (mA/cm²)
Voltage (V)
2
0
-2
-4
-6
-8
-0.2
0.0
0.2
0.4
0.6
0.8

Figure S1. *J-V* characteristic curves of the fabricated OPSCs showing the effect of loading amounts of (a) B-AuQDs, (b) G-AuQDs and (c) R-AuQDs in PEDOT:PSS layer of OSCs

Table S1. The photovoltaic/electrical parameters of fabricated OSCs

	J_{SC} (mA/cm^2)	V_{OC} (V)	FF	%η
Reference cells	6.8±0.1	0.60±0.01	0.59±0.01	3.25±0.03
R-AuQDs				
1.00 μM	7.03±0.04	0.610±0.004	0.570±0.009	3.28±0.02
2.00 μM	6.99±0.06	0.608±0.002	0.590±0.004	3.343±0.002
3.00 μM	6.86±0.04	0.61±0.01	0.603±0.002	3.35±0.03
4.00 μM	6.7±0.2	0.604±0.005	0.583±0.003	3.1±0.1
G-AuQDs				
1.00 μM	6.99±0.08	0.596±0.002	0.605±0.003	3.36±0.04
2.00 μM	7.3±0.3	0.609±0.006	0.58±0.02	3.45±0.02
3.00 μM	7.2±0.2	0.618±0.002	0.604±0.007	3.59±0.03
4.00 μM	7.19±0.07	0.607±0.001	0.59±0.01	3.45±0.05
B-AuQDs				
1.00 μM	6.93±0.04	0.599±0.003	0.593±0.004	3.28±0.04
2.00 μM	6.92±0.03	0.605±0.002	0.589±0.005	3.29±0.03
3.00 μM	6.855±0.008	0.610±0.001	0.585±0.002	3.262±0.003
4.00 μM	6.71±0.07	0.610±0.002	0.579±0.003	3.16±0.03

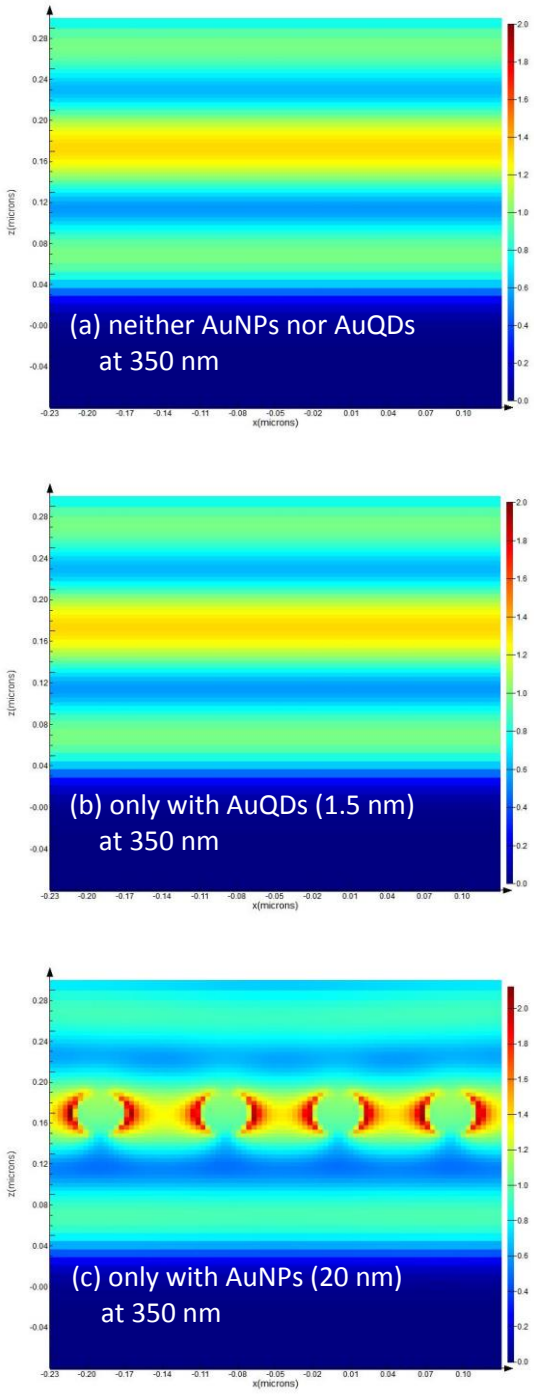

Figure S2. FDTD simulations of OSCs containing (a) neither AuQDs nor AuNPs, (b) OSCs with only AuQDs and (c) OSCs with only AuNPs at illumination light wavelength of 350 nm.

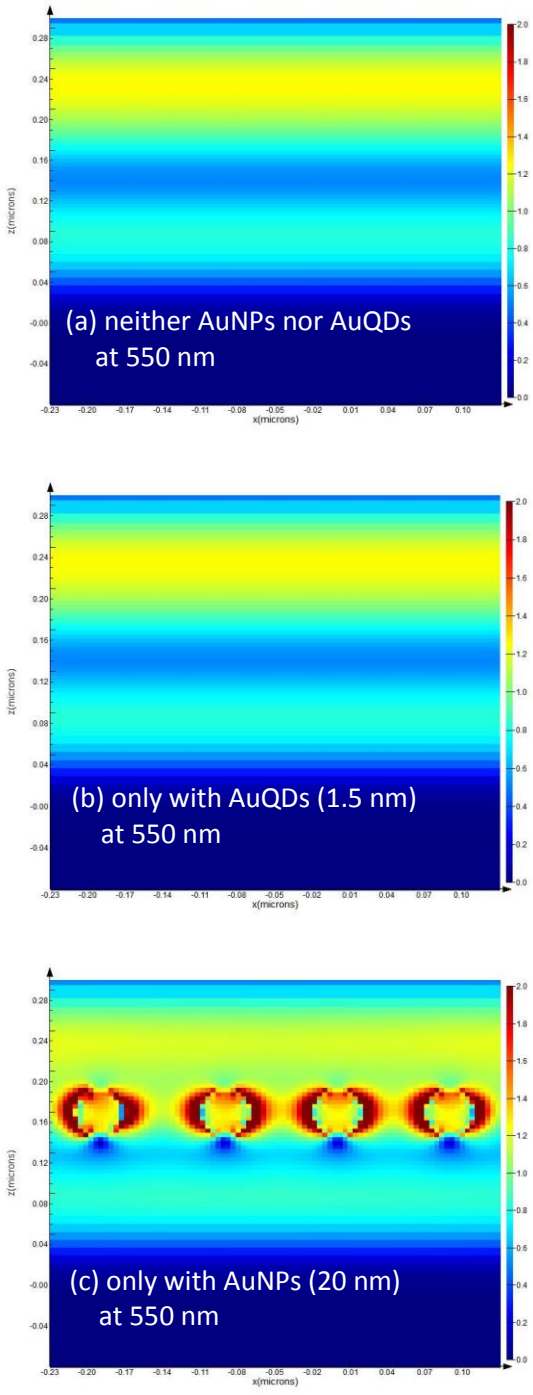

Figure S3. FDTD simulations of OSCs containing (a) neither AuQDs nor AuNPs, (b) OSCs with only AuQDs and (c) OSCs with only AuNPs at illumination light wavelength of 550 nm.

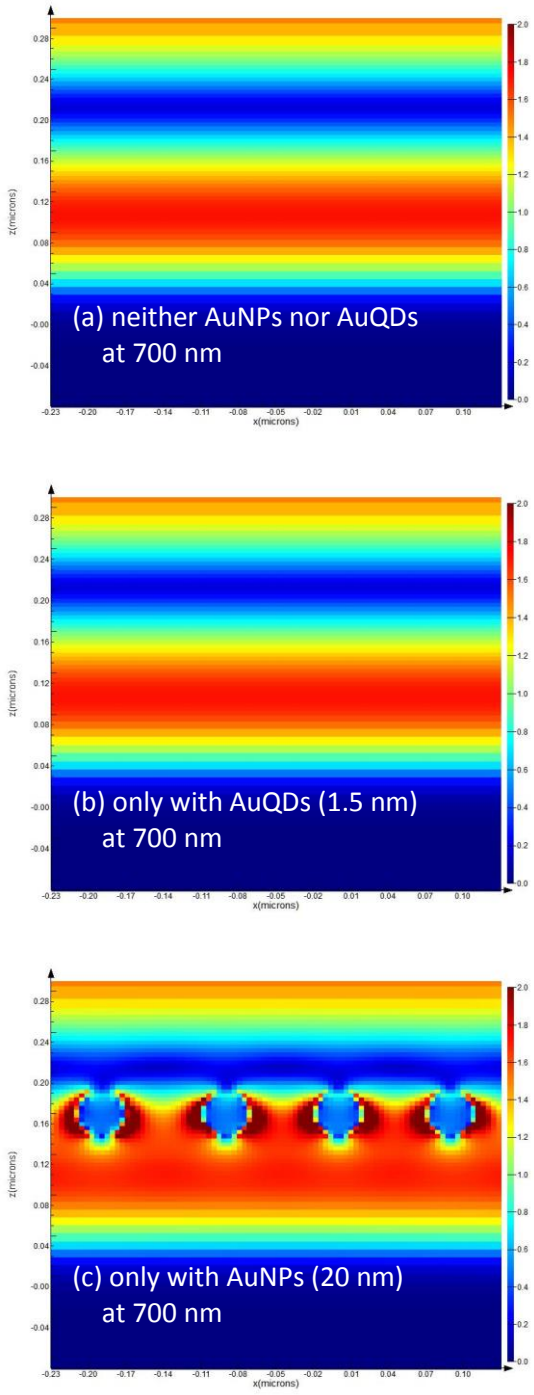

Figure S4. FDTD simulations of OSCs containing (a) neither AuQDs nor AuNPs, (b) OSCs with only AuQDs and (c) OSCs with only AuNPs at illumination light wavelength of 700 nm.

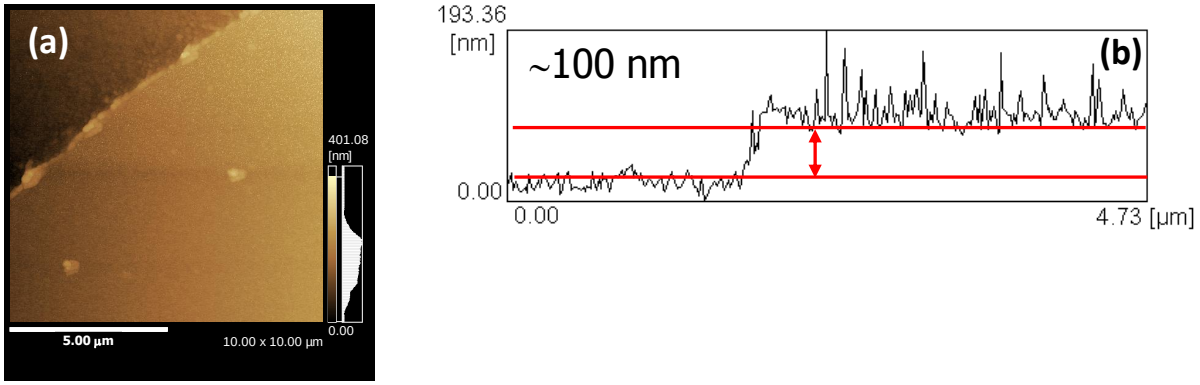

Figure S5. (a) an AFM image and (b) its cross-section profile of a PEDOT:PSS film on an ITO glass substrate indicating the thickness of the film.

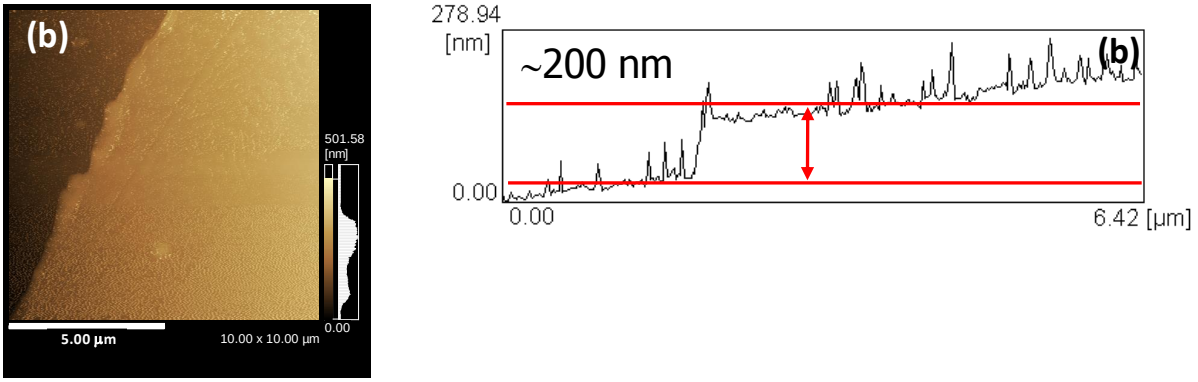

Figure S6. (a) an AFM image and (b) its cross-section profile of P3HT:PCBM/PEDOT:PSS film on an ITO glass substrate indicating the thickness of the film.

APPENDIX C

SUPPORTING INFORMATION FOR CHAPTER IV

Enhanced Organic Thin-Film Solar Cell Efficiency via the Combination of three difference plasmonic excitations of silver nanoprisms (AgNPrs)

(a)

		Level				
		-1.68	-1	0	1	1.68
AgNPrs (mM)	Red	0.00	0.02	0.05	0.08	0.10
	Purple	0.00	0.02	0.05	0.08	0.10
	Blue	0.00	0.02	0.05	0.08	0.10

(b)

Points	AgNPrs		
	Red	Purple	Blue
1	1	1	1
2	1	1	-1
3	1	-1	1
4	1	-1	-1
5	-1	1	1
6	-1	1	-1
7	-1	-1	1
8	-1	-1	-1
9	0	0	-1.682
10	0	0	1.682
11	0	-1.682	0
12	0	1.682	0
13	-1.682	0	0
14	1.682	0	0
15	0	0	0
16	0	0	0
17	0	0	0
18	0	0	0
19	0	0	0
20	0	0	0

Table S1. (a) Experimental design as 3 factors, 3 Level was considered by central composite design (CCD). (b) Coded factor corresponds to concentration of AgNPs in three difference types of size and shape.

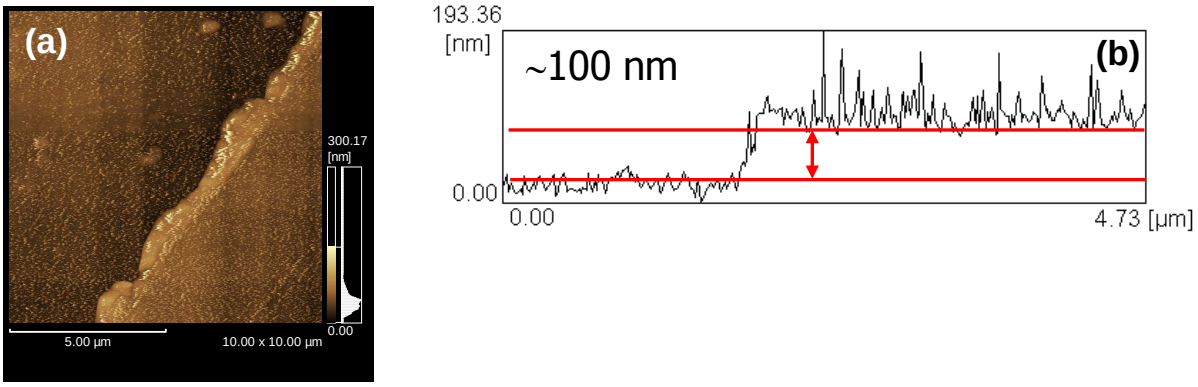

Figure S1 (a) AFM images of scratched PEDOT:PSS film on ITO glass and (b) height profile of PEDOT:PSS film-ITO glass surface. The average thickness is ca. 100 nm.

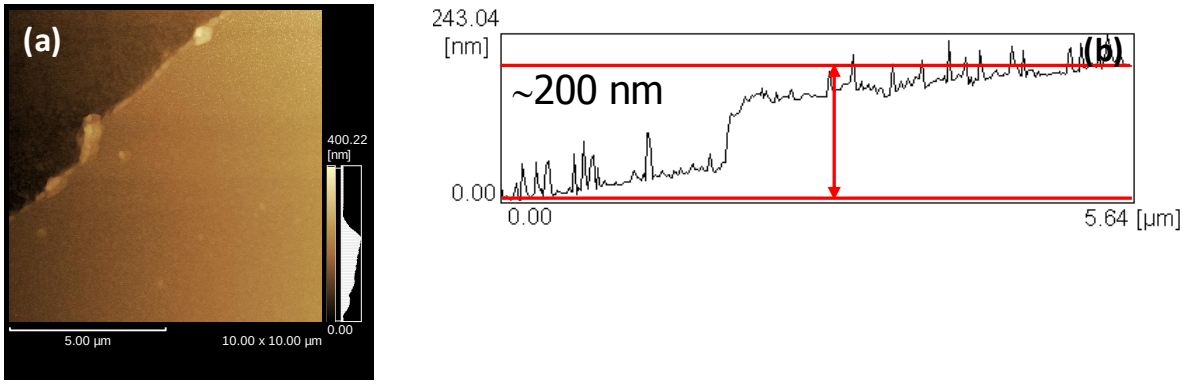

Figure S2 (a) AFM images of scratched P3HT:PCBM/PEDOT:PSS on ITO glass and (b) height profile of P3HT:PCBM/PEDOT:PSS-ITO glass surface The average thickness of P3HT:PCBM/PEDOT:PSS films is ca. 200 nm.

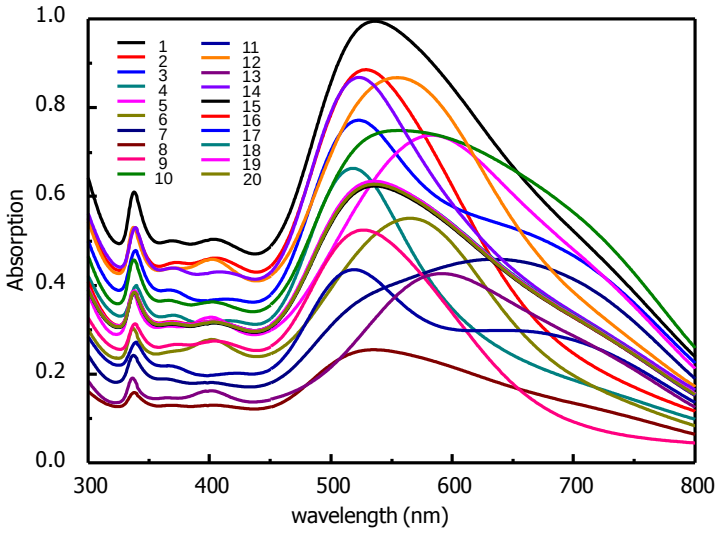

Figure S3 The UV-vis spectra of three differences size and shape of AgNPs were mixed as 20 concentration ratio as follows table 1s.

Table S2. Experimental design as 3 factor, 3 Level and respond (peak area) was considered by central composite design (CCD).

Experimental run	Coded level			Peak area (400 - 650 nm)
	Red	Purple	Blue	
1	1	1	1	190.27
2	1	1	-1	156.97
3	1	-1	1	141.34
4	1	-1	-1	107.04
5	-1	1	1	133.13
6	-1	1	-1	99.02
7	-1	-1	1	82.97
8	-1	-1	-1	48.59
9	0	0	-1.682	90.08
10	0	0	1.682	148.55
11	0	-1.682	0	77.52
12	0	1.682	0	163.76
13	-1.682	0	0	70.64
14	1.682	0	0	152.30
15	0	0	0	118.53
16	0	0	0	119.46
17	0	0	0	119.48
18	0	0	0	119.81
19	0	0	0	120.02
20	0	0	0	118.90

Table S3. The highest peak area compares results between calculation and experiment.

AgNPrs (coded/ concentrations (mM))			Peak area (400 – 650 nm)	
Red	Purple	Blue	Prediction	Experiment
1.682/ 0.10	1.682/ 0.10	1.682/ 0.10	233.2	240.02

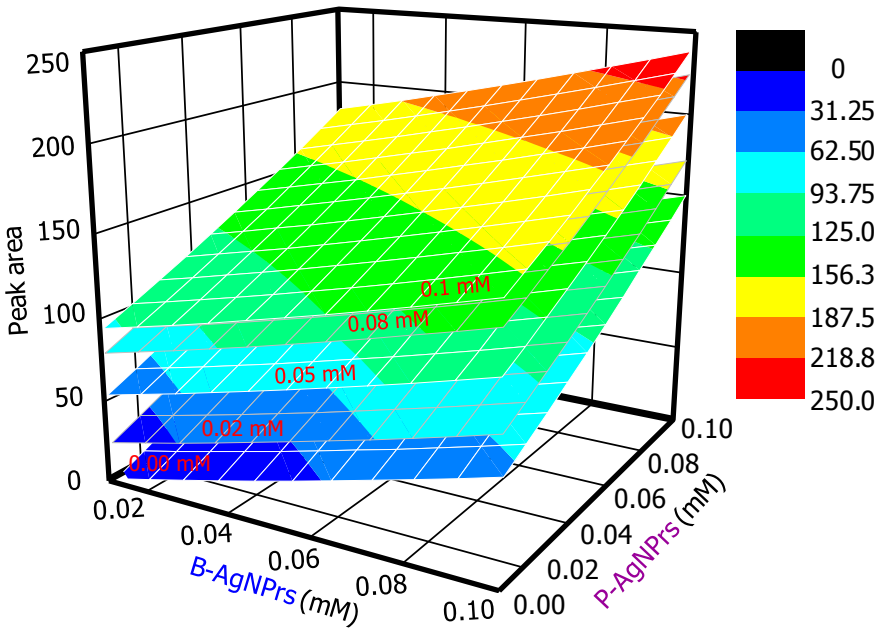

Figure S4 Estimation of response surface of the peak area from 400 – 650 nm of UV-vis spectrum was plotted the concentration of B-AgNPrs and P-AgNPrs from 0 to 0.1 mM with superimposition of surface layers, which represent different concentration of R-AgNPs.

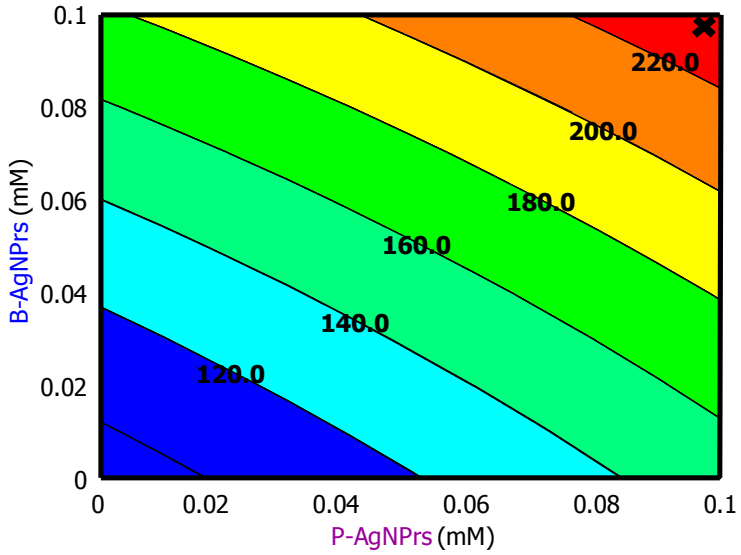

Figure S5 Estimation of response surface of the peak area from 400 – 650 nm of UV-vis spectrum was plotted the concentration of B-AgNPrs and P-AgNPrs from 0 to 0.1 mM with superimposition of surface layers, which represent concentration of R-AgNPrs 0.1 mM.

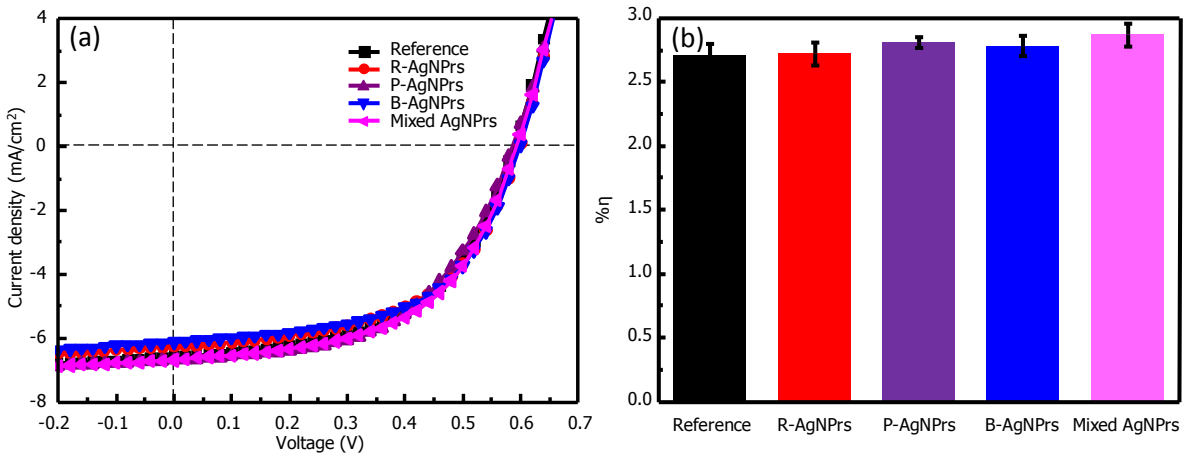

Figure S6 (a) J-V properties of reference cell without AgNPrs, R-AgNPrs, P-AgNPrs, B-AgNPrs and Mixed AgNPrs in PEDOS:PSS layer (using AgNPrs 0.03 mM for all developing OSCs) and (b) the solar cell efficiency (%η) of each OSC.

APPENDIX D

A. CONFERENCES

1. Apichat Pangdam, Kazunari Shinbo, Keizo Kato, Futao Kaneko, Chuchaat Thammacharoen, Sanong Ekgasit and Akira Baba "Properties of Organic Thin Film Solar Cells Fabricated with Urchin-like Gold Nanoparticles" (oral presentation) **JSAP-Hokuriku-Shinetsu regional meeting**, 7-8 November 2014, University of Toyama, Toyama, JAPAN

2. Apichat Pangdam, Kazunari Shinbo, Keizo Kato, Futao Kaneko, Chuchaat Thammacharoen, Sanong Ekgasit and Akira Baba "Effect of Urchin-Like Gold Nanoparticles in Organic Polymer Solar Cells" (poster presentation) **ICNME 2014**, 17-19 December 2014, Kobe, JAPAN

3. Apichat Pangdam, Jing Yang, Jiabao Li, Kazunari Shinbo, Keizo Kato, Futao Kaneko, Chuchaat Thammacharoen, Minghui Hong, Sanong Ekgasit and Akira Baba "Effect of Nanopiller Height on Plasmonic Organic Polymer Solar Cells Fabricated by Thermal Nanoimprinting Technique" (oral presentation) **IEICE General Conference**, 10-13 March 2015, Kyoto, JAPAN

4. Apichat Pangdam, Kazunari Shinbo, Keizo Kato, Futao Kaneko, Chuchaat Thammacharoen, Sanong Ekgasit and Akira Baba "Improving the Efficiency of Plasmonic Organic Solar Cells via Urchin-Like Gold Nanoparticles" (poster presentation) **The 63rd JSAP Spring Meeting 2016**, 19-22 March 2016, Tokyo, JAPAN

5. Apichat Pangdam, Kazunari Shinbo, Keizo Kato, Futao Kaneko, Ryousuke Ishikawa, Chutiparn Lertvachirapaiboon, Chuchaat Thammacharoen, Sanong Ekgasit and Akira Baba "Application of Urchin-Like Gold Nanoparticles (UL-AuNPs) for Light Tapping in Polymer Solar Cells" (oral presentation) **ISOME 2016**, 18-20 May 2016, Niigata, JAPAN

6. Apichat Pangdam, Kazunari Shinbo, Keizo Kato, Futao Kaneko, Ryousuke Ishikawa, Chuchaat Thammacharoen, Sanong Ekgasit and Akira Baba "Enhanced Organic Thin-Film

Solar Cell Efficiency via the Combination of Three Different Silver nanoparticles (AgNPs)" (poster presentation) **JSAP-Hokuriku-Shinetsu regional meeting**, 15-16 July 2016, Ishikawa, JAPAN

7. Apichat Pangdam, Kazunari Shinbo, Keizo Kato, Futao Kaneko, Ryousuke Ishikawa, Chutiparn Lertvachirapaiboon, Sanong Ekgasit and Akira Baba "The effect of gold quantum dots for improving organic thin-film solar cells" (oral presentation) **KJF-ICOMEP 2016**, 4-7 September 2016, Fukuoka, JAPAN

B. PUBLICATIONS

1. **Pangdam, A**.; Nootchanat, S.; Ishikawa, R.; Shinbo, K.; Kato, K.; Kaneko, F.; Thammacharoen, C.; Ekgasit, S.; Baba, A., Effect of Urchin-Like Gold Nanoparticles in Organic Thin-Film Solar Cells. *Physical Chemistry Chemical Physics* **2016**, *18*, 18500 - 18506.

2. **Pangdam, A**.; Nootchanat, S.; Ishikawa, R.; Shinbo, K.; Kato, K.; Kaneko, F.; Lertvachirapaiboon, C.; Ekgasit, S.; Baba, A., Investigation of Gold Quantum Dots Enhanced Organic Thin Film Solar Cells. *ACS Applied Materials & Interfaces* Submitted.

3. **Pangdam, A**.; Nootchanat, S.; Ishikawa, R.; Shinbo, K.; Kato, K.; Kaneko, F.; Lertvachirapaiboon, C.; Wongravee, K; Ekgasit, S.; Baba, A., Enhanced Organic Thin-Film Solar Cell Efficiency via the Combination of Three Difference Plasmonic Excitations of Silver Nanoprisms (AgNPrs). *Physical Chemistry Chemical Physics* Submitted.

VITAE

Name: Mr. Apichat Pangdam; **Date of Birth:** 14 December 1986

Address: 67/1 M.6, Sai Khueng, Phrasaeng, Surat Thani, 84210, THAILAND

E-mail: apichat.pangdam@gmail.com

Education:

2017 Ph.D. (Electrical and Electronic Engineering, Niigata University, JAPAN)

2009 Bachelor of Science (Chemistry, Prince of Songkla University, THAILAND)

Scholarship:

The “Global Circus” Program of Niigata University supported by the Ministry of Education, Culture, Sports, Science and Technology, JAPAN.